Applied Energy 390 (2025) 125871

Contents lists available at ScienceDirect

Applied Energy

journal homepage: www.elsevier.com/locate/apenergy

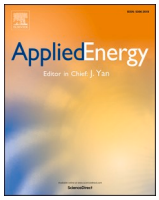

Techno-economic analysis of ammonia to hydrogen and power pathways considering the emerging hydrogen purification and fuel cell technologies

Du Wen [a,*], Xinyi Wei [a,b], Antonin Bruneau [c], Aris Maroonian [c], François Maréchal [a], Jan Van herle [b]

[a] Industrial Process and Energy Systems Engineering, Swiss Federal Institute of Technology in Lausanne (EPFL), Rue de l'Industrie 17, Sion 1951, Switzerland
[b] Group of Energy Materials (GEM), Swiss Federal Institute of Technology in Lausanne (EPFL), Rue de l'Industrie 17, Sion 1951, Switzerland
[c] Neology Hydrogen SA, Lutry 1095, Switzerland

HIGHLIGHTS

- High-temperature ammonia cracker achieves 87.55 % efficiency compared to 86.75 % of low-temperature cracker.
- Using PSA has a higher efficiency penalty but has the lowest LCOH of 2.81 USD/kg.
- SOFC-based system has the highest efficiency of 69.55 % and the lowest LCOE of 0.145 USD/kWh.
- Scaling up to 2000 kg/h ammonia input significantly lowers LCOH and LCOE.
- Ammonia facilitates low-cost hydrogen transport from renewable rich regions to high energy cost markets.

ARTICLE INFO

Keywords:
Ammonia
Decomposition
Fuel cells
Energy storage
Techno-economic analysis

ABSTRACT

Ammonia serves as a promising hydrogen carrier and energy storage medium due to its high hydrogen content, ease of transport, and well-established production infrastructure. This study presents a comprehensive techno-economic analysis of ammonia-to-hydrogen (A2H) and ammonia-to-power (A2P) pathways, comparing various process configurations for hydrogen production and power generation. High-temperature ammonia crackers (600 °C) achieve a maximum energy efficiency of 87.55 % and a maximum exergy efficiency of 86.09 %, outperforming lower-temperature crackers (450 °C), which have energy efficiencies ranging from 82.16 % to 86.75 %. Among hydrogen separation technologies, temperature swing adsorption (TSA) incurs the lowest efficiency penalty but at the highest cost, while pressure swing adsorption (PSA) is more energy-intensive but has the lowest levelized cost of hydrogen (LCOH) at 2.81 USD/kg. In the A2P pathway, the integrated system of the high-temperature cracker and solid oxide fuel cell (SOFC) achieves the highest efficiency of 69.55 % and the lowest levelized cost of electricity (LCOE) at 0.145 USD/kWh, underscoring the crucial role of system efficiency in determining LCOE. Conversely, directly combusting hydrogen in a steam Rankine cycle (SRC) results in the lowest efficiency of 33.2 % and the highest LCOE of 0.715 USD/kWh, making it the least viable option. Furthermore, integrating ammonia with existing energy infrastructures creates new opportunities for hydrogen production and power generation. The results highlight ammonia's potential as a cost-effective hydrogen carrier, particularly in renewable-rich regions for large-scale ammonia synthesis and export to high energy cost markets. This study offers insights into optimal strategies for deploying ammonia-based energy solutions, informing future technological developments and policy frameworks for a hydrogen-driven future economy.

1. Introduction

The global dependence on fossil fuels, derived from the Earth's limited resources, raises concerns about long-term energy security and sustainability. As carbon-based fuels remain the primary energy source, the availability and sourcing of carbon must be reassessed to ensure a resilient energy future. Among various alternatives, hydrogen has garnered significant attention as a clean fuel due to its high energy density and zero direct carbon emissions [1]. However, its widespread

* Corresponding author.
E-mail address: du.wen@epfl.ch (D. Wen).

https://doi.org/10.1016/j.apenergy.2025.125871
Received 28 February 2025; Received in revised form 3 April 2025; Accepted 3 April 2025
Available online 7 April 2025
0306-2619/© 2025 The Authors. Published by Elsevier Ltd. This is an open access article under the CC BY license (http://creativecommons.org/licenses/by/4.0/).

Nomenclature

Symbols

A_{PEMFC}	membrane area of PEMFC, (cm^2)
dA	membrane area of the discrete compartment, (m^2)
E_0	cell potential, (V)
E_{loss}	overpotential loss, (V)
E_{PEMFC}	reversible overpotential of PEMFC, (V)
F	Faraday constant, ($C{\cdot}mol^{-1}$)
$\dot{N}_{H_2}$	hydrogen consumption rate, ($mol{\cdot}s^{-1}$)
$J_{n,\ i}$	cross-membrane flux of component *i* in the compartment n, ($mol{\cdot}m^{-2}{\cdot}s^{-1}$)
J_{PEMFC}	current density of PEMFC, ($A{\cdot}cm^{-2}$)
$k_{1,i}$	extended Langmuir adsorption isotherm parameters, (−)
P_{feed}	feed pressure, (Pa)
Per_i	permeance of component *i*, ($mol{\cdot}m^{-2}{\cdot}s^{-1}{\cdot}pa^{-1}$)
P_i	partial pressure of component i, (bar)
$P_{permeate}$	permeate pressure, (Pa)
Q_f	input feed flow, ($mol{\cdot}s^{-1}$)
Q_p	output permeate flow, ($mol{\cdot}s^{-1}$)
Q_r	output retentate flow, ($mol{\cdot}s^{-1}$)
Q_{fn}	feed flow rate to compartment n, ($mol{\cdot}s^{-1}$)
Q_{pn}	permeate flow rate out of compartment n, ($mol{\cdot}s^{-1}$)
Q_m	retentate flow rate out of compartment n, ($mol{\cdot}s^{-1}$)
q_i	equilibrium amount adsorbed of component i, ($mol{\cdot}kg^{-1}$)
T	operating temperature of the bed, (K)
T_{PEMFC}	operating temperature of PEMFC, (K)
$x_{fn,i}$	feed flow's mole fraction of component i in the compartment n, (−)
$x_{jn,i}$	cross-membrane flux's mole fraction of component i in the compartment n, (−)

Abbreviations

B2A2P	biomass-to-ammonia-to-power
CCGT	combined cycle gas turbine
H2ICE	hydrogen internal combustion engine
HEN	heat exchange network
LCOE	levelized cost of electricity
LCOH	levelized cost of hydrogen
NPV	net present value
P2A2P	power-to-ammonia-to-power
PEMFC	proton exchange membrane fuel cell
PSA	pressure swing adsorption
SRC	steam Rankine cycle
SOFC	solid oxide fuel cell
TSA	temperature swing adsorption

adoption faces storage and transportation challenges, particularly its low volumetric energy density and the need for cryogenic or high-pressure containment systems. While many countries are investing in renewable hydrogen production, not all regions have the geographic, economic, or infrastructural conditions needed to efficiently produce hydrogen from renewable sources. In this context, ammonia has emerged as a promising alternative, offering advantages in hydrogen storage, transport, and utilization. Additionally, cracking imported ammonia provides access to hydrogen as a fuel or feedstock without the need for expensive hydrogen liquefaction and transport, facilitating a globally integrated hydrogen economy. This approach supports the energy transition by extending hydrogen supply chains beyond regions rich in renewables, thereby enhancing energy security across industrial and transportation sectors.

Despite its advantages, ammonia is not a direct fuel and requires conversion through cracking or electrochemical processes to release hydrogen for power generation technologies. A variety of ammonia-to-power conversion technologies has been investigated, including conventional systems such as combined cycle gas turbines (CCGT) and internal combustion engines (ICE), as well as emerging technologies like solid oxide fuel cells (SOFC) and proton exchange membrane fuel cells (PEMFC). Each of these conversion routes offers distinct advantages and challenges regarding efficiency, operating conditions, catalyst stability, emissions, and techno-economic feasibility. Therefore, assessing current research advancements, identifying existing knowledge gaps, and evaluating the feasibility of ammonia as a sustainable energy carrier is crucial for its integration into a global clean energy transition.

This study aims to contribute to this understanding by thoroughly analyzing recent advancements in ammonia-based energy conversion technologies. It will provide a detailed assessment of efficiency, cost, and system performance and explore key research priorities for industrial applications and academic investigations. The findings will guide strategic decisions on ammonia's role in future energy systems and highlight pathways for further technological development and industrial implementation.

1.1. Ammonia cracking

Using ammonia as an energy carrier is widely discussed in terms of technical and economic. Lan et al. conducted a techno-economic analysis comparing pathways for hydrogen-ammonia energy conversion and integrating renewable energy into the power sector [2]. Their study assessed pipeline transmission and High Voltage Alternating Current transmission for hydrogen, ammonia, and hybrid hydrogen-ammonia storage. The findings revealed that hybrid hydrogen-ammonia storage was most economically viable, with a net present value (NPV) of 39.31 million USD and a levelized cost of electricity (LCOE) of 0.081 USD/kWh. In contrast, ammonia-only storage had an NPV of 20.11 million USD, while hydrogen-only storage resulted in a negative NPV due to high storage costs. Wen et al. analyzed power-to-ammonia-to-power (P2A2P) and biomass-to-ammonia-to-power (B2A2P) pathways for carbon neutrality scenarios [3]. The research indicated that B2A2P attained greater efficiencies (40–50 %) relative to P2A2P (27–47 %). Even though B2A2P had a higher CAPEX of 603.3–675.1 million USD, compared to 159.2–181.1 million USD in P2A2P, it offered a shorter payback period of 6 years and a superior NPV of 415.5 million USD. These results highlight ammonia's potential as a fuel and energy storage medium in renewable energy systems.

Ammonia cracking technologies have gained significant attention because direct ammonia fuel has a lower technical readiness level. Recent studies have focused on optimizing catalysts, integrating processes, and improving energy efficiency to enhance ammonia decomposition at scale, making it a viable solution for hydrogen supply chains. Cho et al. conducted a computational fluid dynamics study to examine scale-up challenges in ammonia cracking, focusing on thermo-fluid stability and heat transfer efficiency [4]. Their model revealed that non-uniform temperature distribution caused localized inefficiencies, adversely affecting hydrogen purity. The study demonstrated that using ruthenium (Ru) catalysts lowered activation energy, significantly enhancing reaction kinetics. A pilot-scale system, operating at 450 °C with $Ru/La–Al_2O_3$ catalyst and Pd/Ta composite separation membranes, achieved 99.99 % hydrogen purity and a 99 % ammonia conversion rate, highlighting its potential for industrial-scale implementation.

While catalyst selection plays a crucial role in ammonia cracking

efficiency, large-scale deployment hinges on techno-economic feasibility, particularly regarding process integration and cost competitiveness. Realpe et al. examined the repurposing of methane steam reformers for ammonia cracking with an optimized Co-Ba-Ce catalyst [5]. Their study revealed that without heat integration, ammonia cracking achieved an efficiency of 65.7 %, whereas incorporating adiabatic pre-cracking and heat recovery improved the efficiency to 75.3 %. The levelized cost of hydrogen (LCOH) of centralized ammonia-based hydrogen production was estimated at 5.50 USD/kg, with potential reductions through catalyst enhancements and integrated separation technologies. Makhloufi et al. performed a techno-economic analysis of large-scale ammonia decomposition for high-purity hydrogen production [6]. The ammonia-to-hydrogen plant showed a thermal efficiency of 68.5 %, generating 200 metric tons of hydrogen per day at 250 bar. The study indicated an LCOH of 5.65 USD/kg, with projections suggesting a decrease to 3 USD/kg by 2040, depending on sustained declines in renewable electricity costs and ammonia production.

1.2. Hydrogen purification

Ammonia cracking generates a hydrogen-rich gas that contains residual ammonia, nitrogen, and other impurities. This gas requires a purification step before usage. Pressure swing adsorption (PSA), temperature swing adsorption (TSA), and membrane separation are commonly examined separation technologies. PSA is the most established method for hydrogen purification due to its high selectivity, cost-effectiveness, and scalability. Park et al. evaluated a multi-bed PSA system for hydrogen recovery, demonstrating that a four-bed PSA process using activated carbon and zeolite achieved 99 % hydrogen purity with a recovery rate of up to 82.6 % [7]. Their findings indicated that a series PSA configuration, where adsorption beds operate sequentially, provided higher hydrogen purity than parallel configurations, although it resulted in lower productivity. Similarly, Rahimpour et al. optimized a layered PSA system, achieving 99.99 % hydrogen purity with a 75 % recovery rate, which could be further improved to 80 % under optimized cycle conditions [8].

TSA offers an alternative purification method, especially suited for ultra-pure hydrogen applications. Vo et al. developed a three-bed TSA system using zeolite optimized through machine learning techniques [9]. Their study demonstrated that integrating TSA with hydrogen PSA tail gas for energy recovery significantly enhanced system performance. It achieved low NH_3 concentrations while maintaining operational costs of 162.33 USD per ton of NH_3. The energy consumption was reported at 2174.8 MJ per ton of NH_3, representing only 0.98 % of the LCOH. These results highlight TSA's capability to produce ultra-pure hydrogen for fuel cells, although its lower productivity remains a limitation. Fatemi et al. conducted a comparative analysis of PSA, vacuum swing adsorption (VSA), and TSA for hydrogen purification [10]. Their findings indicated that PSA re-pressurized with product gas achieved 99.99 % hydrogen purity, but low recovery rates diminished its economic viability. Conversely, TSA achieved similar hydrogen purity with minimal CO contamination but required significant heating energy (45.2 MJ/kg H_2) for regeneration, which decreased overall system efficiency. Despite its limitations, TSA remains a viable application option.

Membrane separation has emerged as a promising method for hydrogen purification after ammonia cracking, offering high selectivity and potential integration with fuel cell systems. Compared to the conventional PSA method, membranes allow for continuous separation with lower energy requirements. Jo et al. developed a membrane reactor using a Pd/Ta composite membrane integrated with a Ru/La-Al_2O_3 catalyst, demonstrating in-situ hydrogen extraction during ammonia decomposition [11]. Their study reported that the Pd/Ta membrane achieved over 99.9 % hydrogen purity at 450 °C under a pressurized ammonia feed of 6.5 bar. The membrane reactor also enhanced ammonia conversion efficiency, reaching 99.5 % at 450 °C while eliminating the need for additional purification units. Similarly, Wei et al. investigated zeolitic imidazolate framework (ZIF) membranes for separating ammonia from hydrogen and nitrogen [12]. The membranes achieved an ammonia permeance of 1727 GPU, indicating their potential for selective ammonia removal prior to hydrogen utilization. However, the study noted that hydrogen's higher diffusivity posed a challenge to separation efficiency, necessitating further optimization of membrane materials and operating conditions.

1.3. Ammonia-based power generation

Ammonia, as a standalone fuel, has the disadvantages of toxicity, corrosivity, low flame speed, combustion instability, and challenges such as misfires and high emissions. To address these issues, ammonia is converted into hydrogen to enhance combustion performance. ICE can operate without purification, which improves efficiency and reduces costs. Wang et al. studied ammonia/hydrogen fuel mixtures in ICE, evaluating their combustion performance and emissions across different inlet temperatures [13]. Their research indicated that at an inlet air temperature of 476 K with a 30 % hydrogen blending ratio, combustion stability was enhanced. Increasing hydrogen content improved flame propagation speed and peak heat release rate; however, excess hydrogen (>50 %) led to increased NO_X emissions, necessitating optimized ammonia/hydrogen blending strategies. Their findings suggest that hydrogen/ammonia dual-fuel engines are a viable zero-carbon combustion solution, provided there is precise control of mixture ratios and inlet conditions.

Pankratov et al. [14] numerically investigated the feasibility of integrating urea (an ammonia derivative) reforming with ICE. The proposed system comprises a urea reformer converting urea-water solution to ammonia and subsequently hydrogen, coupled with a spark-ignition engine and auxiliary burner. Despite partial conversion due to high energy requirements, the integrated urea reforming and ICE system achieved an indicated efficiency of 46 %, compared to 42.5 % using natural gas. The study emphasized urea's advantages as a non-toxic, transportable, and carbon-capturing energy carrier, although challenges such as carbon presence and the need for onboard reforming were noted. The research highlights the importance of optimizing reformer design, catalyst efficiency, and thermal management to realize urea's full potential as a sustainable fuel option for ICE applications.

Aside from ICE applications, ammonia has been explored as a fuel for large-scale power plants, particularly in CCGT systems. Richard et al. conducted a techno-economic analysis of ammonia cracking technologies for large-scale power generation applications using hydrogen/ammonia blends in CCGT [15]. This study compared two ammonia cracking methods: membrane reactors and conventional fired tubular reactors. The results showed that integrating the membrane reactor enhanced overall thermal efficiency by over 25 % and reduced LCOH by approximately 10 %. However, the high cost of ammonia remained the predominant factor influencing the LCOE, constituting roughly 80 % of the total. Furthermore, the analysis highlighted critical drawbacks associated with the widespread use of membrane reactors, particularly the scarcity and high cost of essential materials such as palladium and ruthenium. The authors emphasized the need for future research to focus on alternative membrane materials and catalysts to address these resource limitations and unlock the full potential of ammonia cracking in decarbonizing electricity production.

Cesaro et al. analyzed the LCOE of ammonia-based power plants [16]. The study estimated that ammonia-fueled CCGT achieves 38–42 % efficiency while blending 70 % NH_3 with 30 % H_2 boosts efficiency to 42–48 %. Furthermore, they found that at power plant utilization rates below 25 %, ammonia becomes cost-competitive with other low-carbon dispatchable technologies, including carbon capture and storage and nuclear power. The LCOE estimates for ammonia-based power generation varied from 70 to 120 USD/MWh, depending on efficiency levels and ammonia prices. Sánchez et al. further explored ammonia's

thermochemical conversion by investigating an ammonia-fueled CCGT system with a catalytic membrane reactor for hydrogen separation [17]. Their findings showed that pre-cracking ammonia before combustion enhanced system performance, with the optimal NH_3/H_2 blending (70 % NH_3 / 30 % H_2) improving ignition characteristics and reducing NO_X emissions, which pose a significant challenge in direct ammonia combustion. Their ammonia-to-power facility achieved a total efficiency of about 40 %, primarily limited by the gas turbine's temperature cap of 1600 °C. They estimated that the costs of producing ammonia-based electricity range from 0.2 to 0.6 EUR/kWh, depending on renewable electricity prices and improvements in electrolyzer efficiency.

SOFC can directly operate on ammonia, benefiting from its high-temperature decomposition (600–1000 °C) into hydrogen and nitrogen. Ammonia-fed SOFCs can achieve efficiencies of up to 57 %, which is comparable to hydrogen-fed SOFCs [18]. Mukelabai et al. investigated a P2A2P system utilizing a reversible solid oxide cell (rSOC) integrated with the Haber-Bosch ammonia synthesis process [19]. The results revealed that the round-trip efficiency of the system varied from 41 % to 53 %, depending on ammonia production rates. The optimized system attained an electricity consumption of 6.4–8.21 kWh/kg NH_3, making ammonia a feasible energy storage solution for intermittent renewable energy. Al-Hamed and Dincer proposed an ammonia-powered SOFC system for locomotives, incorporating onboard hydrogen production through waste heat utilization in an SOFC-gas turbine hybrid system [20]. Their thermodynamic analysis indicated that the system achieved an overall energy efficiency of 61.2 % and an exergy efficiency of 66.3 %. The results indicated that ammonia-fed SOFCs represent a promising pathway for zero-emission railway transportation, although further optimization of waste heat utilization and reformer efficiency is necessary.

However, low electrochemical reaction rates related to ammonia directly restrict the achievable power densities when compared to hydrogen-fueled SOFCs. Ammonia decomposition variation within the SOFC can lead to inconsistent OCV, affecting overall efficiency. What's more, anode degradation caused by nickel nitride formation remains a critical challenge, necessitating the pre-decomposition of ammonia before SOFC operation [21]. Sánchez et al. assessed ammonia as a hydrogen carrier for fuel cells, evaluating their viability for direct use versus hydrogen extraction before application [22]. The results indicated that while direct operation of fuel cells with ammonia is feasible, the efficiency remains lower than that of using hydrogen. Specifically, integrated ammonia cracking and SOFC configuration achieved an overall efficiency of 40 %, while direct ammonia SOFCs were limited by conversion losses and material degradation. The study also estimated electricity production costs at 700 EUR/MWh for the ammonia cracking option and 1200 EUR/MWh for direct use.

Peng et al. benchmarked an SOFC-ammonia power generation system, emphasizing that efficiency is crucial for cost competitiveness [23]. While electrolysis-based decomposition remains at TRL 1–2 due to high material costs and durability limitations, their study indicated that ammonia-fueled SOFC could achieve efficiencies of up to 60 %, provided that anode degradation is mitigated. Further advancements in direct ammonia-fed SOFC have been explored to enhance efficiency and address degradation issues. Elmutasim et al. reviewed both experimental and computational developments, reporting that the highest power density achieved for SOFC is at 650 °C [24]. Their study also identified that hydrogen spillover from Ni to the Ni-YSZ interface has the lowest activation barrier, improving reaction kinetics. Despite achieving an efficiency of 50 %, SOFC systems continue to face performance limitations due to nickel nitridation and microstructural deformation, necessitating anode surface modifications and the development of alternative catalysts.

PEMFC represents another viable technology for utilizing ammonia as a hydrogen carrier. Although PEMFC requires high-purity hydrogen, which necessitates ammonia decomposition and hydrogen separation, it offers lower operating temperatures and faster startup times compared to SOFC, making it suitable for distributed and residential energy applications. Pinzón et al. conducted a simulation of an ammonia-to-power system designed for residential use, where ammonia was first decomposed, followed by hydrogen separation for either PEMFC or direct hydrogen combustion [25]. Without optimization, the system exhibited an efficiency of 36 %, but integrating a heat exchanger network increased efficiency to 46 %, demonstrating the potential for process enhancements. Their economic analysis further highlighted that producing hydrogen from ammonia (0.54 USD/kg) was significantly cheaper than storing pure hydrogen (14.95 USD/kg), reinforcing ammonia's feasibility as part of a circular hydrogen economy. The study emphasized the importance of waste heat recovery and advanced separation techniques in maximizing efficiency.

The viability of ammonia as an energy carrier goes beyond individual conversion technologies to include broader system-level comparisons between conventional combustion-based methods and non-conventional fuel cell-based approaches. Mucci et al. conducted a model-based evaluation of ammonia energy storage systems, comparing three power-to-ammonia and ammonia-to-power pathways: (i) ammonia thermal decomposition with fuel cell conversion, (ii) ammonia decomposition via auto-thermal reforming, and (iii) ammonia direct combustion in combined power cycles. Their findings demonstrated that roundtrip efficiency ranged from 30 % to 34 %, with the fuel cell-based system being the most efficient [26]. The LCOE varied between 0.28 and 0.31 EUR/kWh, assuming a renewable electricity purchase price of 0.03 EUR/kWh.

1.4. Gaps and contributions

Ammonia has emerged as a promising energy carrier, particularly because of its ease of storage and transportation and the various pathways available for its production [27,28]. This versatility makes ammonia an appealing candidate for integration into the energy and industry sectors. However, considering profitability, not all countries and districts are suitable for using ammonia as the hydrogen/energy carrier. Previous studies have not adequately discussed conditions such as technology selection and varying electricity market prices, which are correlated with system efficiency and levelized cost. A trade-off can be made according to the downstream requirement.

In this study, the ammonia-to-hydrogen (A2H) and ammonia-to-power (A2P) pathways are formulated by considering two types of crackers and relevant catalysts, three hydrogen purification technologies: PSA, TSA, and membrane, and four power generation technologies through combustion with SRC, H2ICE, PEMFC, and SOFC. The techno-economic performance of each configuration serves as the primary evaluation metric. Instead of identifying a single optimal technological pathway, this study aims to highlight the trade-offs among different options, providing industry insights into selecting the most suitable route under various conditions. Additionally, it examines how advancements in TRL and scalability factors could change the viability of different ammonia-based energy pathways, offering a forward-looking perspective on the future development of energy systems. The contributions of this study are (1) providing the conditions of using ammonia as the hydrogen/energy carrier through the A2H pathway to compete with on-site hydrogen production; (2) integrating hydrogen power generation technologies in the A2P pathway and optimizing the system efficiency; (3) identifying the significant factors influencing the LCOH and LCOE and highlighting future efforts.

2. Materials and methods

This section first defines the scope and boundaries of the work, including a description of A2H and A2P pathways. Then, it introduces the technologies involved and the specific details needed to construct process models. Finally, in the scenario analysis, all configurations are evaluated using key performance indicators to find the optimal solution.

2.1. System description

Fig. 1 illustrates the schematic diagram for the ammonia-to-hydrogen (A2H) and ammonia-to-power (A2P) pathways. Ammonia is imported from countries that offer competitive prices for green ammonia because of their abundant renewable energy resources and capabilities for large-scale transportation. Initially, the ammonia is pressurized by a pump and sent to an ammonia cracker, where it is heated to a high temperature to decompose into hydrogen and nitrogen with the help of catalysts. The resulting gas from the cracker first expands in a turbine to recover energy and is then cooled before entering a gas cleaning unit (scrubber), where water removes unreacted ammonia. The stripped ammonia can either be further recovered or treated as wastewater. The remaining hydrogen and nitrogen are separated using membrane, PSA, or TSA technologies. After purification, hydrogen is compressed to 350 bar and delivered to end users, while the retentate flow is burned in a burner. The heat flows in the system are optimized by a heat exchanger network (HEN) connected to a steam Rankine cycle (SRC) to recover available energy.

The A2H pathway involves using H2ICE, PEMFC, and SOFC to generate electricity, with heat as a byproduct. The purity of hydrogen is restricted for PEMFC, especially for the unreacted ammonia, which must be reduced to parts per million levels before entering PEMFC to avoid material degradation. In contrast, there are no strict requirements for SOFC and H2ICE, allowing the separation process to be omitted. The gases produced by the cracker are injected into the SOFC and H2ICE after adjusting the pressure and temperature to satisfy the necessary conditions. Subsequently, the off-gas is also directed to the burner. Moreover, the resulting gas can be burned directly, providing heat to HEN to integrate a SRC. It should be noted that devices such as heaters, coolers, pumps, compressors, and turbines are used to meet the temperature and pressure requirements of different processes. They are not shown in the figure for the sake of simplicity.

2.2. System modeling

2.2.1. Ammonia cracker

The imported ammonia at 25 °C and 15 bar is first pressurized to 20 bar through a pump to meet the pressure requirement of the ammonia cracker. After that, it is heated to a high temperature and sent to the cracker, where the ammonia decomposition reaction (Eq. (1)) occurs with the help of catalysts. This endothermic reaction is temperature-dependent, requiring a high reaction temperature for an efficient conversion rate. The thermodynamic conversion of ammonia primarily depends on the temperature within the medium range of 250–450 °C, while the conversion rate plateau occurs at temperatures above 450 °C [29]. At these high temperatures, the reaction kinetics are crucial for achieving near 100 % conversion. The specific reactor design and catalyst selection are beyond the scope of this work; thus, an RGibbs reactor in ASPEN Plus V.11 [30] is utilized to represent maximum forward reaction progress. Experimental results from the reference [31] confirm that the reaction above 450 °C can achieve thermodynamic equilibrium conversion.

$$2NH_3 \rightarrow N_2 + 3H_2, \Delta H_0 = 92.44 kJ/\text{mol} \quad (1)$$

The influence of catalysts and their respective reactor designs mainly affects reactor temperature and, subsequently the cost estimation. In lab-scale experiments, the ruthenium (Ru) catalyst is costly and requires a relatively lower operating temperature of 450 °C to attain a high conversion rate, whereas the iron (Fe) catalyst is more economical but operates at a higher temperature of 600 °C. A trade-off must be considered when evaluating the technical and economic performance of these two types of catalysts. The catalyst's decomposition activity and the volumetric flow rate of the inlet gas are used to estimate the total amount of catalyst required. The catalyst chosen based on experimental results aligns with the simulation in terms of operating temperature and exhibits a similar conversion rate. After the cracker, the gas mixture is directed to a scrubber to remove ammonia for downstream applications, particularly PEMFC. The technical parameters of the ammonia cracker and scrubber are presented in Table 1.

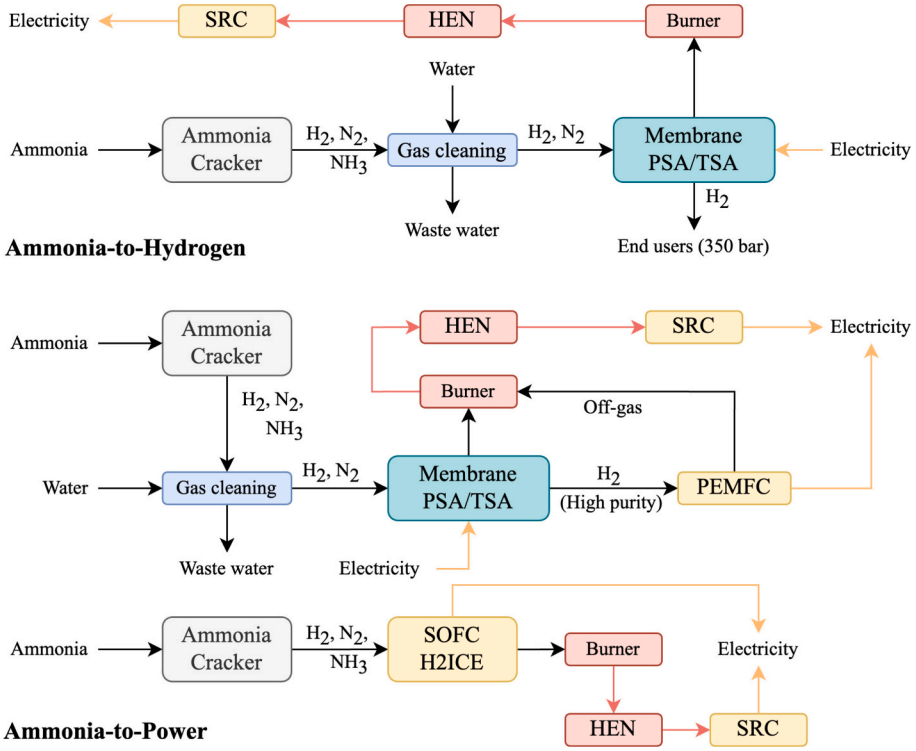

Fig. 1. Schematic diagram of the ammonia-to-hydrogen and ammonia-to-power pathways.

Table 1
Technical parameters of the ammonia cracker [15].

Name	Value	Unit
Input mass flow rate	1000	$kg{\cdot}h^{-1}$
Reactor type	RGibbs	
Operating temperature	600/450	°C
Operating pressure	20	bar
Conversion rate	98.1/91.9	%
Working pressure of the scrubber	5	bar
Pump efficiency	0.9	–
Compressor isentropic efficiency	0.8	–
Turbine isentropic efficiency	0.7	–
Mechanical efficiency	0.9	–
Decomposition activity of Ru catalyst [29]	9000	$ml{\cdot}h^{-1}{\cdot}g_{cat}^{-1}$
Decomposition activity of Fe catalyst [29]	6500	$ml{\cdot}h^{-1}{\cdot}g_{cat}^{-1}$

2.2.2. Hydrogen separation and purification

A two-dimensional discrete membrane model is constructed based on reference [32], as shown in Fig. 2(a). Due to differences in pressure and concentration, the feed flow Q_f is pressurized and enters the membrane, where it divides into permeate flow Q_p and retentate flow Q_r. An analytical model has been developed to determine the permeate and retentate flows using Eqs. (2)–(9). In each compartment, the cross-membrane flux $J_{n,\,i}$, is calculated first, taking into account the components' permeance, pressure difference, and concentration difference, as demonstrated in Eq. (2). Permeance indicates the difficulty of a component passing through the membrane; thus, it is preferable to have high permeance for hydrogen and low permeance for nitrogen, and vice versa. The ratio of the permeance of the two components defines the membrane's selectivity, which is another crucial characteristic. The retentate flow Q_{rn}, which serves as the feed flow for the next compartment, is determined by subtracting the permeate flow Q_{pn} from the feed flow. The retentate flow in the last compartment represents the final output retentate flow from this membrane. The permeate flow is the total of the cross-membrane flows across all compartments.

Some assumptions are made: 1. There is no mixing along the permeate channel. The difference in chemical potential between the two compartments, which creates a partial pressure gradient that drives gas transport, is not considered; 2. The separation process is isothermal; 3. The pressure drops on both the feed and permeate sides of the membrane are deemed negligible; 4. The permeance of gas components is pressure-independent, enabling linear modeling of cross-membrane flux; 5. The model assumes cross-plug flow, indicating that the concentration on the feed side varies incrementally along the length of the membrane, while the permeate mixes immediately after passing through the membrane; 6. Concentration polarization effects are neglected, resulting in a uniform concentration on both sides of the membrane.where $J_{n,i}$ is the cross-membrane flux of component i in the compartment n, $mol{\cdot}m^{-2}{\cdot}s^{-1}$; Per_i is the permeance of component i, $mol{\cdot}m^{-2}{\cdot}s^{-1}{\cdot}pa^{-1}$; P_{feed} and $P_{permeate}$ are the feed and permeate pressure, respectively, pa; $x_{fn,i}$ is the feed flow's mole fraction of component i in the compartment n, –; $x_{jn,i}$ is the cross-membrane flux's mole fraction of component i in the compartment n, –. After calculating the cross-membrane flux of each compartment, the retentate and permeate flows are determined accordingly:

$$Q_{pn} = \sum_i J_{n,i} dA \tag{3}$$

$$Q_{rn} = Q_{fn} - \sum_i J_{n,i} dA \tag{4}$$

$$Q_{fn} = Q_{r(n-1)}, X_{fn,i} = X_{r(n-1),i} \tag{5}$$

where Q_{pn} is the permeate flow rate out of compartment n, $mol{\cdot}s^{-1}$; dA is the membrane area of the discrete compartment, m^2; Q_{rn} is the retentate flow rate out of compartment n, $mol{\cdot}s^{-1}$; Q_{fn} is the feed flow to compartment n, which equals to retentate flow rate $Q_{r(n-1)}$ from previous compartment n-1, $mol{\cdot}s^{-1}$; $X_{fn,i}$ is the mole fraction of the feed flow to compartment n, which equals to that of the retentate flow ($X_{r(n-1),i}$) from pervious compartment n-1, –; The boundary conditions in the retentate channel depend on the first and last compartments are:

$$Q_f = Q_{f0}, Q_r = Q_{rn} \tag{6}$$

$$X_{f,i} = X_{f0,i}, X_{r,i} = X_{rn,i} \tag{7}$$

where Q_f is the input feed flow rate, $mol{\cdot}s^{-1}$; Q_{f0} is the feed flow rate of the first compartment 0, $mol{\cdot}s^{-1}$; Q_r is the output retentate flow rate, $mol{\cdot}s^{-1}$; Q_{rn} is the retentate flow rate of the last compartment n, $mol{\cdot}s^{-1}$; $X_{f,i}$ is the mole fraction of the input feed flow, –; $X_{f0,i}$ is the mole fraction of the feed flow in the first compartment 0, –; $X_{r,i}$ is the mole fraction of the output retentate flow, –; $X_{rn,i}$ is the mole fraction of the retentate flow in the last compartment n, –. It uses a different method to decide the boundary conditions of the permeate channel:

$$Q_p = \sum_n Q_{pn} \tag{8}$$

$$X_{p,i} = \frac{\sum_n Q_{pn} X_{pn,i}}{Q_p} \tag{9}$$

where Q_p is the output permeate flow rate, $mol{\cdot}s^{-1}$; Q_{pn} is the permeate flow rate of each compartment, $mol{\cdot}s^{-1}$; $X_{p,i}$ is the mole fraction of the output permeate flow, –; $X_{pn,i}$ is the mole fraction of permeate flow in each compartment, –.

Fig. 2(b) illustrates the configuration of the membrane system, which incorporates two membranes along with auxiliary devices such as compressors and heat exchangers. The upstream flow is cooled to 35 °C, which falls within the economically optimal operating temperature

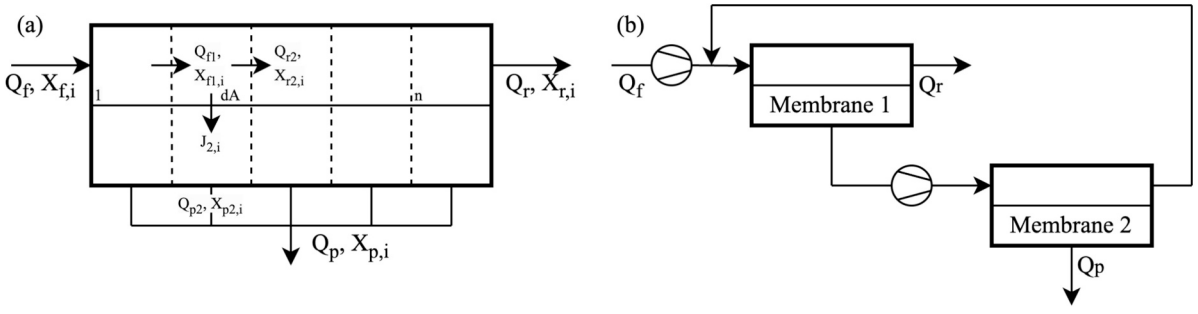

Fig. 2. Schematic diagram of the membrane model and membrane system configuration.

$$J_{n,i} = Per_i\left(P_{feed}x_{fn,i} - P_{permeate}x_{jn,i}\right) \tag{2}$$

range for a compressor. It is then pressurized before passing through the membrane. The choice of pressure represents a trade-off between membrane area and the compressor's energy consumption, which can be dictated by the project's objectives. The first stage of the membrane has concentrated most of the required substance; however, one membrane alone is insufficient to meet the purity standards. The retentate flow exits the membrane system, while the permeate flow proceeds to the second stage of the membrane, which is modeled similarly. The permeate flow is directed to storage, while the retentate flow is returned for circulation or sent to the burner. Table 2 outlines the assumptions used for the membrane model. It is important to note that the characteristics of the membranes vary significantly due to the different materials and processing technologies. Metallic, polymeric, graphite, and ceramic membranes each have their own advantages and disadvantages [33]. A commercial membrane [34] with relatively higher permeability and electrical efficiency is utilized in this work.

PSA and TSA are also considered for hydrogen/nitrogen separation. The PSA and TSA models are built upon reference [10], where the dynamic model has been further simplified. A mathematical approach is applied for both technologies, explicitly formulating only the mass balance. In contrast, the electricity, heating, and cooling needed for the adsorption and desorption processes rely on the operating conditions and are estimated in the process model. The extended Langmuir model is employed to predict adsorption equilibrium for the gas mixture:

$$q_i = \frac{q_{mi} B_i P_i}{1 + \sum_{i=1}^{n} B_i P_i} \tag{10}$$

$$q_{mi} = k_{1,i} + k_{2,i} T \tag{11}$$

$$B_i = k_{3,i} exp\left(\frac{k_{4,i}}{T}\right) \tag{12}$$

where q_i is the equilibrium amount adsorbed of component i, mol·kg^{-1}; P_i is the partial pressure of component i, bar; T is the operating temperature of the bed, K; $k_{1,i}$, $k_{2,i}$, $k_{3,i}$, and $k_{4,i}$ are extended Langmuir adsorption isotherm parameters.

Both PSA and TSA systems contain four beds to enable consecutive hydrogen separation and purification operations, as the adsorption and de-adsorption processes require time, particularly for cooling in TSA technology. The adsorption and de-adsorption duration is 90 s for both technologies, but TSA necessitates an additional 270 s for cooling. Consequently, the operating time of one bed using TSA is four times longer than that of using PSA. The extended Langmuir model defines the adsorbent's capacity at specific temperature and pressure conditions. In this work, these are determined by the subsequent process. Based on the flow rate of the gas mixture and its compositions, the amount of adsorbent per second is estimated while considering a target purity. Subsequently, the total quantity of adsorbent and, therefore, the bed volume can be calculated using density and porosity. It is important to note that the cooling duty of the bed is estimated based on the specific heat of the adsorbent. Table 2 presents the assumptions for PSA and TSA.

Some assumptions are made: 1. Fluid dynamics and pressure drop in the bed are considered negligible; only mass balance is strictly regarded. 2. The operation is isothermal, with no heat exchange between the gas, adsorbent, and bed. The adsorbent and bed are heated or cooled to match the temperature of the gas mixture before it enters the bed. 3. Lumped mass transfer is treated differently, with the amount of adsorbent and bed volume determined by the time required to reach isothermal adsorption equilibrium and the input flow rate. 4. The capacity of the adsorbent depends on temperature and pressure, with adsorption temperature and pressure aligned with the upcoming ammonia cracking process, while the de-adsorption temperature and pressure are at ambient levels. 5. A longer cooling time is considered, as a shorter cooling time would require a higher cooling duty or a more efficient heat exchange design, leading to increased costs. 6. The heating, cooling, and electricity consumption of the operation are calculated within process models.

Table 2
Technical parameters of membrane [34,35], PSA and TSA [10].

Name	Value	Unit
Membrane type	Polymer	
Working temperature	35	°C
Feed pressure	6.5	bar
H_2 permeability	10–1000	GPU
Selectivity between H_2 and N_2	100–1000	–
Adsorption isotherm parameters of H_2	4.314/−0.0106/0.002515/458	–
Adsorption isotherm parameters of N_2	4.813/0.0067/5.695E-04/1531	–
Zeolite density	1160	kg·m^{-3}
Zeolite specific heat	920	J·kg^{-1}·K^{-1}
Zeolite porosity	0.65	–
Bed porosity	0.357	–

2.2.3. Hydrogen power generation

PEMFC, SOFC, H2ICE, and SRC are considered for power generation in the A2P pathway. Analytical models are used in process simulation, with the PEMFC model based on references [36, 37]. According to the Nernst equation, the reversible overpotential can be estimated:

$$E_{PEMFC} = E_0 + \frac{R T_{PEMFC}}{2F} ln\left(\frac{P_{H_2}\sqrt{P_{O_2}}}{P_{H_2O}}\right) \tag{13}$$

$$E_0 = 1.299 - 0.000846(T_{PEMFC} - 298.15) \tag{14}$$

where E_{PEMFC} is the reversible overpotential, V; E_0 is the cell potential, V; R is the ideal gas constant, J·mol^{-1}·K^{-1}; T_{PEMFC} is the working temperature, K; F is the Faraday constant, C·mol^{-1}; P_{H_2}, P_{O_2}, and P_{H_2O}, are the partial pressure, respectively, kPa. It should be noted that the overpotential losses (activation, ohmic, and concentration) are estimated by the measured potential from experiments and the calculated result. The power generation of PEMFC is determined by the reversible overpotential and current density:

$$P_{PEMFC} = (E_{PEMFC} - E_{loss}) J_{PEMFC} A_{PEMFC} \tag{15}$$

$$J_{PEMFC} A_{PEMFC} = 2F\dot{N}_{H_2} \tag{16}$$

where E_{loss} is the overpotential loss, V; J_{PEMFC} is the current density, A·cm^{-2}; A_{PEMFC} is the membrane area, cm^2; $\dot{N}_{H_2}$ is the hydrogen consumption rate, mol·s^{-1}. It is important to note that a single-pass fuel utilization rate of 83 % is used to estimate the hydrogen consumption rate in the fuel cell.

To ensure a long PEMFC lifetime, high purity of hydrogen (99.9 %) should be maintained, as nitrogen negatively affects stack performance [38]. The SOFC model is formulated using a similar analytical framework [39], and there is no strict hydrogen purity requirement. Table 3 presents the assumptions for both PEMFC and SOFC. In PEMFC and SOFC, cooling water and swept air are utilized, respectively, to maintain the operating temperature. Since the SOFC has no strict purity requirements, 80 % of the exhaust gas is recycled back to the stack, while the remainder is directed to the afterburner. The H2ICE model is built according to reference [40]. A black-box method is used, where the resulting gas from the cracker is injected into the combustion chamber along with air. To improve the engine's performance, combustion stability, and emissions, an air-to-fuel equivalence ratio of 2.2 is chosen. This results in an optimal brake thermal efficiency of 41 %.

2.2.4. Energy recovery

The ammonia cracker operates at high temperatures (450 °C - 600 °C) and pressure (20 bar). The gases produced by the crackers

Table 3
Technical parameters of PEMFC [36], SOFC [39], HEN [41], and SRC [42].

Name	Value	Unit
PEMFC		
H_2 purity	99.9	%
Overpotential loss	0.31	V
Current density	0.2	A·cm^{-2}
Operating temperature	65–75	°C
Operating pressure	2	bar
Fuel utilization rate	83	%
SOFC		
Overpotential loss	0.16	V
Current density	0.4	A·cm^{-2}
Operating temperature	680–760	°C
Operating pressure	1	bar
Fuel utilization rate	70	%
HEN		
Cooling water temperature range	15–20	°C
Minimum temperature approach	5	°C
SRC		
High pressure steam turbine inlet pressure	60–200	bar
Medium pressure steam turbine inlet pressure	20–80	bar
Low pressure steam turbine inlet pressure	1.5	bar
Water condensed pressure	0.05	bar

contain significant energy that can be harnessed to enhance system efficiency. Furthermore, waste heat from SOFC, burners, ICE, and multi-stage compressors can also be utilized. This study implements a HEN to effectively manage these hot and cold streams within the system. A framework from a previous study [41] informs the design and optimization of the HEN for a single-period scenario. By considering the hot and cold streams along with their temperature ranges, a mixed integer linear programming problem aimed at minimizing energy consumption is formulated, where mass and energy balances are considered. Additionally, it determines the optimal utility network using heat cascade equations and pinch analysis while also focusing on minimizing investment costs. Following this framework, available and avoidable waste heat is first assessed and transformed into a usable form [43]. Whenever there is available waste heat at temperatures exceeding 250 °C, the system can then integrate a SRC. The integration can be represented as a series of constraints within the mixed integer programming problem outlined in the earlier HEN framework [42]. The design parameters of HEN and SRC are given in Table 3.

2.3. Scenario analysis

Different configurations for A2H and A2P pathways are outlined in Table 4. This study examines two types of crackers for ammonia decomposition. The high-temperature cracker requires cheaper iron catalysts, whereas the relatively low-temperature cracker needs more expensive ruthenium catalysts. Utilizing ruthenium will decrease the heating duty of the cracker, though it is more expensive. The viability of the novel catalyst will be presented in the next chapter. It also explores three separation technologies: membranes, which offer a compact setup but come with higher costs; PSA, which has a high TRL and low cost but higher energy consumption; and TSA, which is ideal for large-scale gas separation, particularly when waste heat is readily available. Concerning the A2P pathway, established PEMFC technology is compared to emerging SOFC technology. PEMFC requires high hydrogen purity and minimal ammonia impurity, necessitating a separation unit and scrubber between the cracker and the fuel cell. In contrast, SOFC tolerates a broader range of inlet gas compositions but is more expensive than PEMFC. Additionally, H2ICE and SRC, where hydrogen is combusted in a combustion chamber, are also considered. These systems can be retrofitted from existing configurations.

Table 4
Different configurations for A2H and A2P pathways.

	Name	Cracker	Separation	Power
A2H	S1	Fix bed (600 °C)	Membrane	–
	S2	Fix bed (600 °C)	PSA	–
	S3	Fix bed (600 °C)	TSA	–
	S4	Membrane reactor (450 °C)	Membrane	–
	S5	Membrane reactor (450 °C)	PSA	–
	S6	Membrane reactor (450 °C)	TSA	–
A2P	S7	Fix bed (600 °C)	Membrane	PEMFC
	S8	Fix bed (600 °C)	PSA	PEMFC
	S9	Fix bed (600 °C)	TSA	PEMFC
	S10	Membrane reactor (450 °C)	Membrane	PEMFC
	S11	Membrane reactor (450 °C)	PSA	PEMFC
	S12	Membrane reactor (450 °C)	TSA	PEMFC
	S13	Fix bed (600 °C)	–	SOFC
	S14	Membrane reactor (450 °C)	–	SOFC
	S15	Fix bed (600 °C)	–	H2ICE
	S16	Membrane reactor (450 °C)	–	H2ICE
	S17	Fix bed (600 °C)	–	SRC
	S18	Membrane reactor (450 °C)	–	SRC

Technical and economic key performance indicators are utilized to identify optimal configurations and are compared with competitors in the market.

Energy efficiency:

$$\eta_{H_2} = \frac{m_{H_2} LHV_{H_2}}{m_{NH_3} LHV_{NH_3} + Q + P_{in}} \tag{17}$$

$$\eta_{ele} = \frac{P_{out}}{m_{NH_3} LHV_{NH_3} + Q} \tag{18}$$

where η_{H_2} is the system energy efficiency when producing hydrogen, −; m_{H_2} is the mass flow rate of the produced hydrogen, kg·s^{-1}; LHV_{H_2} is the lower heating value of hydrogen, MJ·kg^{-1}; m_{NH_3} is the mass flow rate of the consumed ammonia, kg·s^{-1}; Q is external heat, kW; P_{in} is electricity consumption, kW; η_{ele} is the system energy efficiency when producing electricity, −; P_{out} is the electricity produced, kW.

Exergy efficiency:

$$\psi_{H_2} = \frac{m_{H_2} Ex_{H_2}}{m_{NH_3} Ex_{NH_3} + Q\left(1 - \frac{T_a}{T}\right) + P_{in}} \tag{19}$$

$$\psi_{ele} = \frac{P_{out}}{m_{NH_3} Ex_{NH_3} + Q\left(1 - \frac{T_a}{T}\right)} \tag{20}$$

where ψ_{H_2} is the system exergy efficiency when producing hydrogen, −; Ex_{H_2} is the chemical exergy of hydrogen, MJ·kg^{-1}; Ex_{NH_3} is the chemical exergy of ammonia, MJ·kg^{-1}; T_a is ambient temperature, K; T is the required heating temperature, K; ψ_{ele} is the system exergy efficiency when producing electricity, −.

Levelized cost of hydrogen (LCOH) and levelized cost of electricity (LCOE):

$$LCOH = \frac{C_{CAPEX} CRF + C_{OPEX}}{3600 m_{H_2} h} \tag{21}$$

$$LCOE = \frac{C_{CAPEX} CRF + C_{OPEX}}{P_{out} h} \tag{22}$$

$$CRF = \frac{i(1+i)^n}{(1+i)^n - 1} \tag{23}$$

where C_{CAPEX} is the capital expenditure of the system, MUSD; CRF is the capital recovery factor, −; C_{OPEX} is the operational expenditure of the system, MUSD; h is the annual operating hour, h; i is the discount rate, −; n is the lifetime of the system. All assumptions for the cost estimation are shown in **Table 5**.

3. Results and discussion

3.1. Ammonia to hydrogen

In the A2H pathway, two crackers and three separation technologies are examined and compared regarding their technical and economic aspects. The technical performance is outlined in Table 6. Scenarios utilizing the high-temperature cracker (S1, S2, S3) exhibit higher energy and exergy efficiencies than those employing the relatively lower-temperature cracker (S4, S5, S6). The highest recorded energy and exergy efficiencies are 87.55 % and 86.09 %, respectively, in S3 when using TSA for hydrogen separation. Although high-temperature crackers demand more heating duty, which results in an efficiency penalty, energy recovery through a turbine, HEN, and the SRC integration can mitigate this penalty. Additionally, high-temperature operation benefits ammonia decomposition, yielding a higher hydrogen production rate of over 170 kg/h compared to approximately 160 kg/h from a lower-temperature operation. These factors contribute to the high efficiencies observed. When the operating temperature of the cracker decreases from 600 °C to 450 °C, it significantly impacts systems utilizing membrane and PSA, leading to an efficiency penalty of around 4 %, contrasted with 1 % in the system using TSA.

Considering the hydrogen separation process, PSA is the most energy-intensive, followed by membrane and TSA. To maintain the high pressure of the resulting gas after the cracker (20 bar) for an optimal adsorption rate, no turbine is used to recover the energy. In contrast, the operating pressures of TSA and membranes are 1 bar and 6.5 bar, respectively, allowing for more potential energy recovery. As a result, the electricity consumption of scenarios using PSA is double that of TSA. Systems utilizing membranes and PSA produce heat that can be recovered through optimizing the HEN and integrating SRC, leading to modest electricity generation of about 50 kW and further improvements in efficiency. A scrubber purifies hydrogen using water as the adsorbent and is placed in different locations depending on the separation technology used. Because ammonia negatively affects the membrane's lifespan, the scrubber is positioned before membrane separation. To minimize pressure or heat losses during scrubbing, it is located after PSA or TSA, which requires more water.

Fig. 3 illustrates the breakdown of CAPEX and OPEX, while Table 7 presents the specific proportions of each component within the system. The system utilizing TSA in S3 has the highest CAPEX at 12.1 million USD (MUSD). Aside from the fixed proportions of contingency and fee costs (CF) and auxiliary facilities costs (AF), the process vessel contributes the most at 17.8 %, followed by the compressor at 16.4 %, the turbine at 12.5 %, the cracker at 6.4 %, and the adsorbent at 5.2 %. The remainder can be considered negligible. Due to the adsorbent's time-consuming cooling process, the operating time of TEA for each adsorption/de-adsorption cycle is four times longer than that of PSA. Consequently, the size of the process vessel is larger than that of other scenarios to accommodate the same amount of resulting gas from the cracker. Expenditure on the compressor is unavoidable due to the high-pressure hydrogen storage requirement, which is 350 bar. The turbine recovers significant energy from the resulting gas, reducing imported electricity and enhancing system efficiency. However, it constitutes over 10 % of the CAPEX, while electricity represents only 3.5 % of the OPEX. The gain is less than the loss, particularly when electricity prices are low. Additionally, the turbine's outlet pressure is ambient, requiring more adsorbent in the TSA process to achieve a high conversion rate.

The system utilizing membranes in S1 has the second-highest CAPEX of 9.2 MUSD. The compressor comprises 21.5 %, followed by the turbine (9.7 %), HEX (9.5 %), cracker (8.5 %), SRC (5.5 %), and membrane (2.4 %). The costs of compressors are similar, as they compress comparable amounts of hydrogen. However, the cost of the turbine is half that of S3 because, as the outlet pressure of the turbine increases, the output power decreases, further impacting the cost. Available and accessible waste heat is effectively utilized and converted into electricity, although at an additional cost. It is important to note that even though the membrane accounts for only 2.4 % of the CAPEX, its cost is significantly influenced by its performance.

In this study, a membrane with high hydrogen permeance and selectivity between hydrogen and nitrogen has been selected, leading to a reduced membrane area needed to achieve a high hydrogen conversion rate. The membrane cost in Table 5 is derived from pilot or commercial-scale applications, where the production scale lowers its

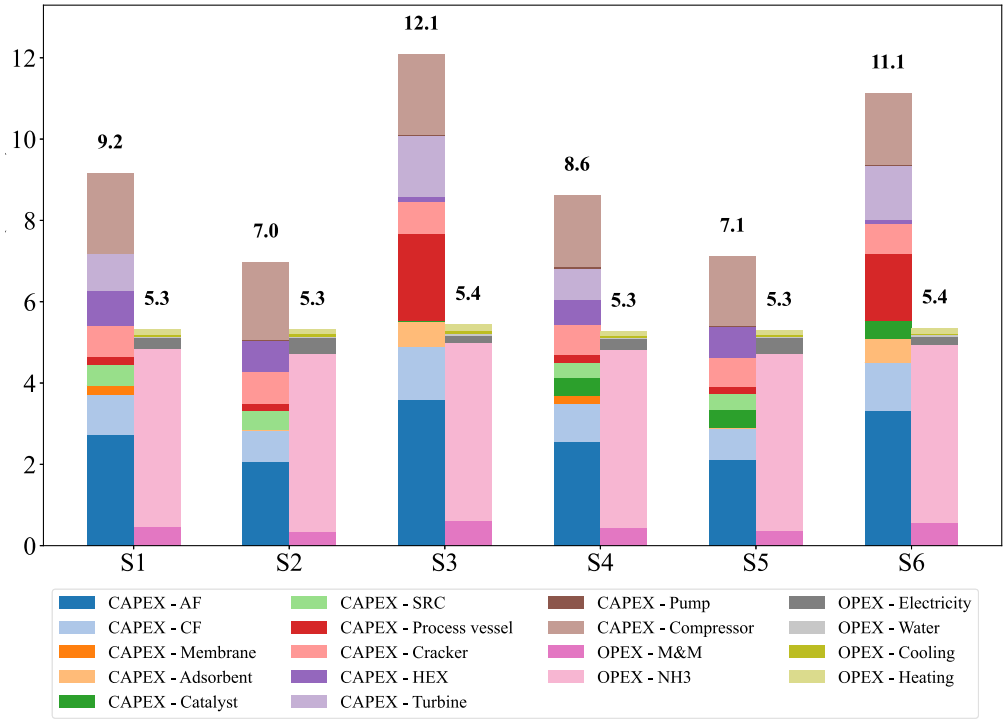

Fig. 3. Breakdown of CAPEX and OPEX of scenarios in the A2H pathway.

Table 5
Assumptions for the cost estimation[1].

Name	Value	Unit	Year	Ref.
Lifetime of the plant	30	y		–
Operating hour per year	8000	hr		–
Discount rate	6	%		–
Maintenance and manpower	5 % of CAPEX			–
PEMFC system cost[2]	1997	USD/kW	2016	[44]
Lifetime of PEMFC	20,000	hr		[44]
SOFC cost[3]	2441	USD/kW	2016	[45]
Lifetime of SOFC	20,000	hr		[45]
ICE cost[4]	1788	USD/kW	2022	[46]
Membrane cost	10–50	USD/m^2	2024	[47]
Lifetime of membrane	5	y		
Zeolite cost[5]	2–10	USD/kg	2021	[48]
Lifetime of zeolite	5	y		[48]
Heating cost	3.51	USD/GJ	2016	[49]
Cooling cost	4.77	USD/GJ	2016	[49]
Water cost	0.53	USD/t	2016	[49]
Ruthenium catalyst cost	500	USD/kg	–	[50]
Lifetime of ruthenium catalyst	5	y		
Iron catalyst cost	10	USD/kg	–	[50]
Lifetime of iron catalyst	5	y		
Electricity price for industrial[6]	0.09 (Min: 0.06, Max: 0.33)	USD/kWh	2024	[51]
Electricity price for commercial[6]	0.14 (Min: 0.09, Max: 0.38)	USD/kWh	2024	[51]
Nitrogen price	0.25	USD/m^3	2022	[52]
Hydrogen price[7]	5.25 (Min: 0.7, Max: 9.8)	USD/kg	2024	[53]
Ammonia price[8]	0.53 (Min: 0.29, Max: 0.98)	USD/kg	2023	[54]

[1] As the data comes from references in different years, inflation should be accounted for using a scaling factor, specifically the Consumer Price Index (CPI) [55].

[2] The cost of the PEMFC, based on a 10-kW system, includes stacks, balance of plant, markup, and installation. The annual manufacturing units are 10,000, which correlates with the cost. Stacks represent 21 % of the total cost.

[3] The cost of the SOFC encompasses stacks, the balance of plant, markup, and installation, derived from a 10-kW system, with annual manufacturing units at 10,000 as well. The system size correlates with the unit cost, where the unit cost of a 100-kW system is half that of a 10-kW system. The size effect should be considered in cost estimation, and stacks account for 7 % to 29 % of the total cost.

[4] H2ICE is an emerging technology, and detailed cost data is currently limited. The cost of H2ICE is assumed to be similar to that of ICE, and the refit cost is not included.

[5] The cost of zeolite correlates with its total weight, indicating that lower weight corresponds to higher cost.

[6] A total average value is utilized. Electricity prices for industrial and commercial uses are applied to the cost of electricity consumption and the revenue from net electricity production, respectively.

[7] The unit is converted from USD/MMBtu (million British thermal units) to USD/kg using the lower heating value of hydrogen, applying an average value of 8.8 USD/MMBtu equals 1 USD/kg.

[8] The unit is converted from USD/short ton to USD/kg. Ammonia prices are influenced by natural gas prices, as ammonia is primarily produced from natural gas.

unit cost. These factors contribute to the small proportion of the membrane in the CAPEX. However, the discussion regarding membrane performance affecting cost is beyond the scope of this work. The system employing PSA in S2 has the lowest CAPEX at 7.0 MUSD. The difference between S2 and S1 arises from the use of a turbine and membrane, which adds an extra 1.1 MUSD. The OPEXs of the various scenarios are similar because over 80 % comes from ammonia, which remains consistent across each scenario. The maintenance and manpower (M&M) cost is estimated using a certain percentage of CAPEX. Electricity and heating comprise about 5 % and 2.5 % of OPEX, respectively.

Fig. 4 illustrates the LCOH distribution across various scenarios in the A2H pathway, taking into account different ammonia prices. The bars represent cases using the average ammonia price of 0.53 USD/kg, while the upper and lower boundaries reflect the maximum price of 0.98 USD/kg and minimum price of 0.29 USD/kg, respectively. Fluctuating electricity prices are not discussed, as they represent only a small portion of the OPEX. Additionally, the maximum and minimum market prices of hydrogen are displayed in Fig. 4 to clarify the position of the A2H pathway. The lowest market price of hydrogen, shown in green, is 0.7 USD/kg, primarily sourced from the chemical sector (mainly ammonia and its derivatives) and refineries. These sectors contribute over 89 % of hydrogen production, benefiting from on-site mass production and utilization, which helps reduce costs. In contrast, the highest market price is 9.8 USD/kg, particularly in the manufacture of electrical equipment, appliances, and components, where higher purity is crucial.

The average LCOH ranges from 4.27 to 4.74 USD/kg. The lowest LCOH, at 2.81 USD/kg, occurs in systems using a high-temperature cracker and PSA for separation, while the highest LCOH, at 7.59 USD/kg, is found in systems using a low-temperature cracker and TSA for separation. Different separation technologies lead to a significant disparity in CAPEX, but the variation in LCOH is not as pronounced as in CAPEX due to the inverse relationship in efficiency. The LCOH is influenced by the energy source, whether from fossil fuels or renewable energy, as well as requirements like purity and storage conditions. Electricity costs represent the largest portion of LCOH when employing water electrolysis. The LCOH from renewable-driven water electrolysis ranged from 3 to 8 USD/kg, according to referenced data [56]. Considering that 1 kg of hydrogen can produce nearly 5.6 kg of ammonia, and given that the lowest LCOH is 3 USD/kg, the cost of ammonia is estimated to exceed 0.53 USD/kg. The lowest ammonia price is achieved with natural gas as the feedstock, making it not directly comparable to the LCOH from renewable sources.

The optimal solution, considering various LCOHs worldwide, is for countries with lower electricity prices, even at zero cost, to leverage their abundant renewable energy for large-scale hydrogen production through water electrolysis, subsequently utilizing ammonia as the hydrogen carrier. Due to the scale effect of production, the LCOH can be further reduced. Additionally, by coordinating the scheduling of electrolysis stacks, the penetration of renewable energy will increase, aiding in their carbon neutrality goals. Ammonia can then be exported to countries with higher electricity prices. In these nations, the LCOH from on-site water electrolysis is high, and using natural gas incurs additional environmental costs, and importing hydrogen requires consideration of transportation costs and safety issues. Therefore, importing ammonia at

Table 6
Technical performance of scenarios in the A2H pathway.

	Ammonia input	Hydrogen output	Water consumption	Electricity consumption	Electricity generation (SRC)	Heating duty	Cooling duty	Energy efficiency	Exergy efficiency
	kg/h	kg/h	kg/h	kW	kW	kW	kW		
S1	1000	172.4	1708.9	459.4	62.3	1060.7	269.0	86.75 %	84.90 %
S2	1000	170.6	6544.2	593.2	54.1	880.7	274.7	86.34 %	83.98 %
S3	1000	174.1	6652.3	261.4	–	1200.7	405.2	87.55 %	86.09 %
S4	1000	161.6	2542.7	450.1	41.2	927.5	190.2	82.83 %	81.48 %
S5	1000	159.9	8461.1	556.1	42.8	807.5	226.1	82.16 %	80.48 %
S6	1000	162.6	8572.7	288.6	–	997.5	187.1	86.75 %	84.90 %

Table 7
Breakdown of CAPEX and OPEX of scenarios in the A2H pathway.

	Compressor	Pump	Turbine	HEX	Cracker	Process vessel	SRC	Catalyst	Adsorbent	Membrane
S1	21.5 %	0.2 %	9.7 %	9.5 %	8.5 %	2.1 %	5.5 %	0.1 %	–	2.4 %
S2	27.5 %	0.1 %	–	11.3 %	11.1 %	2.4 %	6.6 %	0.2 %	0.3 %	–
S3	16.4 %	0.1 %	12.5 %	1.0 %	6.4 %	17.8 %	–	0.1 %	5.2 %	–
S4	20.5 %	0.3 %	8.9 %	7.4 %	8.5 %	2.1 %	4.4 %	5.0 %	–	2.4 %
S5	24.2 %	0.1 %	–	10.6 %	10.3 %	2.3 %	5.5 %	6.1 %	0.3 %	–
S6	15.9 %	0.1 %	12.0 %	0.9 %	6.6 %	14.8 %	–	3.9 %	5.3 %	–

	CF	AF	CAPEX (MUSD)	Heating	Cooling	Water	Electricity	NH_3	M&M	OPEX (MUSD)
S1	10.7 %	29.8 %	9.2	2.6 %	0.9 %	0.2 %	5.4 %	82.3 %	8.6 %	5.3
S2	10.7 %	29.8 %	7.0	2.2 %	0.9 %	0.7 %	7.3 %	82.3 %	6.6 %	5.3
S3	10.7 %	29.8 %	12.1	2.9 %	1.3 %	0.7 %	3.5 %	80.5 %	11.1 %	5.4
S4	10.7 %	29.8 %	8.6	2.3 %	0.6 %	0.3 %	5.6 %	83.0 %	8.2 %	5.3
S5	10.7 %	29.8 %	7.1	2.0 %	0.8 %	0.9 %	7.0 %	82.6 %	6.7 %	5.3
S6	10.7 %	29.8 %	11.1	2.5 %	0.6 %	0.9 %	3.9 %	81.7 %	10.4 %	5.4

Table 8
Technical performance of scenarios in the A2P pathway.

	Ammonia input	Water consumption	Electricity generation	Electricity Generation (SRC)	Heating duty	Cooling duty	Energy efficiency	Exergy efficiency
	kg/h	kg/h	kW	kW	kW	kW		
S7	1000	1708.9	2996.2	343.5	870.7	1000.0	55.32 %	54.59 %
S8	1000	6544.2	2824.2	415.3	870.7	1094.8	53.66 %	52.96 %
S9	1000	6652.3	3227.2	230.4	870.7	1060.6	57.27 %	56.52 %
S10	1000	2542.7	2789.2	309.6	797.5	918.5	51.96 %	51.68 %
S11	1000	8461.1	2647.3	378.9	797.5	996.7	50.74 %	50.47 %
S12	1000	8572.7	2968.6	251.7	797.5	870.5	53.99 %	53.70 %
S13	1000	–	4114.4	203.1	1040.7	268.7	69.55 %	69.09 %
S14	1000	–	3818.0	229.4	967.5	252.2	65.98 %	66.04 %
S15	1000	–	2290.5	964.5	870.7	1839.0	53.91 %	53.21 %
S16	1000	–	2147.1	1053.8	805.5	1987.5	53.60 %	53.32 %
S17	1000	–	343.9	1749.7	870.7	2214.6	34.68 %	34.22 %
S18	1000	–	276.6	1703.2	797.5	2139.0	33.20 %	33.02 %

Table 9
Breakdown of CAPEX and OPEX of scenarios in the A2P pathway.

	Comp.	Pump	Turbine	HEX	Cracker	Burner	Process vessel	SRC	FC/ICE	Catalyst	Adsorbent
S7	1.4 %	0.1 %	5.4 %	11.4 %	4.7 %	11.7 %	1.2 %	9.8 %	12.5 %	0.1 %	–
S8	1.4 %	0.1 %	–	14.1 %	4.9 %	12.2 %	1.1 %	12.6 %	12.9 %	0.1 %	0.2 %
S9	1.1 %	0.1 %	7.4 %	7.2 %	3.8 %	9.4 %	10.5 %	6.9 %	10.1 %	0.1 %	3.1 %
S10	1.3 %	0.2 %	4.7 %	10.1 %	4.5 %	11.8 %	1.1 %	9.8 %	12.2 %	2.7 %	–
S11	1.3 %	0.1 %	–	13.7 %	4.6 %	12.0 %	1.0 %	11.7 %	12.3 %	2.7 %	0.1 %
S12	1.0 %	0.1 %	6.6 %	7.9 %	3.6 %	9.4 %	8.1 %	8.2 %	9.8 %	2.1 %	2.9 %
S13	0.6 %	0.1 %	7.0 %	19.3 %	3.9 %	6.5 %	0.3 %	6.8 %	14.9 %	0.1 %	–
S14	0.5 %	0.0 %	5.8 %	20.2 %	3.4 %	5.9 %	0.3 %	8.0 %	13.3 %	2.0 %	–
S15	–	0.1 %	–	19.4 %	7.8 %	–	–	25.2 %	6.9 %	0.1 %	–
S16	–	0.1 %	–	19.2 %	6.7 %	–	–	23.6 %	6.0 %	3.9 %	–
S17	–	0.0 %-	6.8 %	16.7 %	3.5 %	12.4 %	–	20.1 %	–	0.1 %	–
S18	–	0.0 %-	6.0 %	16.1 %	3.3 %	12.1 %	–	20.1 %	–	1.9 %	–

	Membrane	CF	AF	CAPEX (MUSD)	Heating	Cooling	Water	NH_3	M&M	OPEX (MUSD)
S7	1.3 %	10.7 %	29.8 %	16.5	2.1 %	3.3 %	0.0 %	79.7 %	15.0 %	5.5
S8	–	10.7 %	29.8 %	15.8	2.1 %	3.6 %	0.5 %	79.4 %	14.4 %	5.5
S9	–	10.7 %	29.8 %	20.5	2.0 %	3.3 %	0.5 %	76.3 %	17.9 %	5.7
S10	1.3 %	10.7 %	29.8 %	16.3	1.9 %	3.0 %	0.1 %	80.1 %	14.9 %	5.5
S11	–	10.7 %	29.8 %	16.0	1.9 %	3.3 %	0.7 %	79.5 %	14.6 %	5.5
S12	–	10.7 %	29.8 %	20.4	1.9 %	2.7 %	0.7 %	76.8 %	17.9 %	5.7
S13	–	10.7 %	29.8 %	19.9	2.5 %	0.9 %	–	78.8 %	17.9 %	5.6
S14	–	10.7 %	29.8 %	21.3	2.3 %	0.8 %	–	77.9 %	19.0 %	5.6
S15	–	10.7 %	29.8 %	9.9	2.2 %	6.2 %	–	82.3 %	9.3 %	5.3
S16	–	10.7 %	29.8 %	11.0	2.0 %	6.6 %	–	81.2 %	10.2 %	5.4
S17	–	10.7 %	29.8 %	22.4	1.9 %	6.6 %	–	72.8 %	18.6 %	6.0
S18	–	10.7 %	29.8 %	22.4	1.8 %	6.4 %	–	73.1 %	18.7 %	6.0

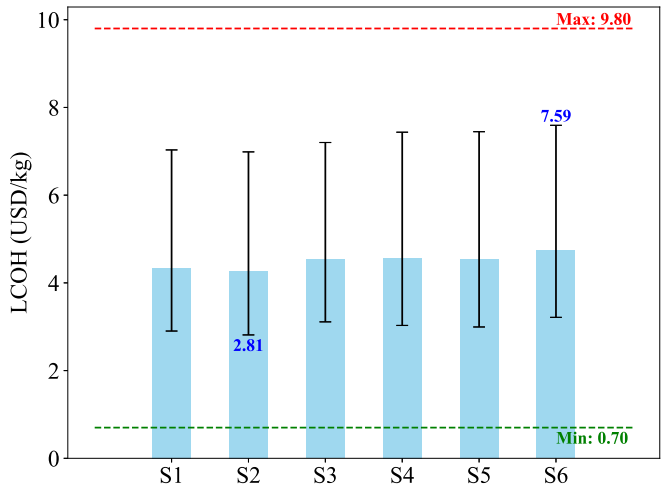

Fig. 4. LCOH distribution of different scenarios in the A2H pathway, considering different ammonia prices.

a low price becomes the most viable solution for them. Based on the electricity price in a country, it can be easily determined whether on-site hydrogen production or ammonia import is more suitable, along with the corresponding pricing.

A sensitivity analysis was conducted for different system sizes, and the relevant LCOH distribution is shown in Fig. 5. As the system size increases, there is an initial sharp decrease in LCOH, after which the slope flattens. The elbow point occurs at 2000 kg of ammonia per hour. Beyond this point, the size effect is not significant, as the decrease in LCOH is around 5 %. In a small-scale system, the configuration using PSA in S2 and S5 has the lowest LCOH, followed by the membrane and TSA technologies. Due to the small cracker, separation technologies dominate the costs at this stage. Conversely, in a large-scale system, the differences between high and low-temperature crackers become more pronounced. Surprisingly, the large-scale system utilizing membranes emerges as the best option compared to PSA or TSA. Although CAPEX is not linearly correlated with size, electricity costs are. As a result, the share of electricity costs in LCOH increases as the system expands. The PSA system consumes more electricity, leading to higher electricity expenses, which makes it less competitive for large-scale applications. TSA could be a viable option for large-scale applications if it can effectively reduce the system size, for instance, by increasing the operating pressure to condense the resulting gas.

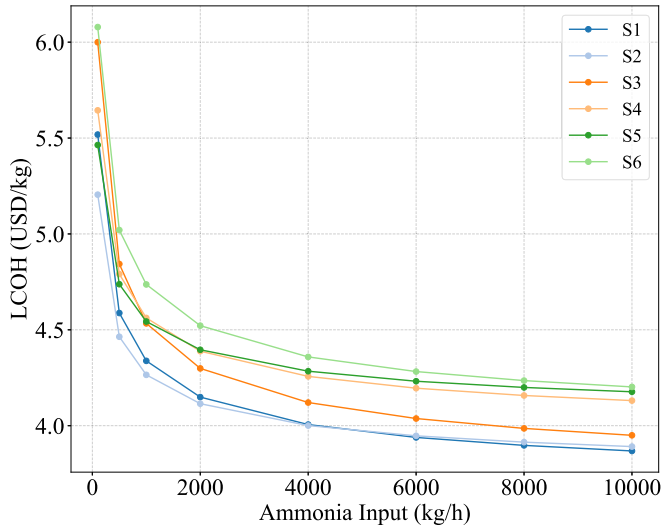

Fig. 5. LCOH distribution regarding different system sizes.

In summary, while using a high-temperature (600 °C) cracker results in a higher CAPEX, the LCOH is lower than that of a low-temperature (450 °C) cracker due to its higher efficiency. The choice of separation technology depends on specific requirements and conditions. The PSA system has the lowest CAPEX and LCOH; however, it is more energy-intensive, resulting in the lowest system efficiency. Conversely, the membrane system is suitable for large-scale applications due to its lower energy consumption. The TSA system, on the other hand, offers the highest efficiency at the greatest cost. A win-win option for the A2H pathway involves producing renewable-driven hydrogen and ammonia in countries with lower electricity prices and selling the ammonia to nations with higher electricity prices. By considering the electricity prices in a country, potential sellers or buyers of ammonia can be identified, aiding in the development of a cost-effective hydrogen production strategy.

3.2. Ammonia to power

In the A2P pathway, ammonia first decomposes into hydrogen. The integration of separation and purification processes is influenced by the fuel requirements of downstream hydrogen-based power generation technologies. Four hydrogen-to-power technologies are discussed and compared in terms of their technical and economic aspects. The efficiency and electricity output are illustrated in Fig. 6, while the remaining results are presented in Table 8.

Scenarios (S13, S14) that integrate SOFC outperform all others in terms of energy and exergy efficiencies and electricity output, followed by those incorporating PEMFC (S7 to S12), H2ICE (S15, S16), and SRC (S17, S18). The highest energy and exergy efficiencies of 69.55 % and 69.09 % occur in scenario S13, respectively. In this scenario, the system employs a high-temperature cracker without separation and purification processes, along with a high-temperature SOFC and an afterburner. Although this requires a higher heating duty from the cracker and SOFC, resulting in an energy penalty, it benefits from an increased hydrogen production rate for downstream power generation and enhanced SOFC efficiency. Electricity generation through SRC is minimal, around 200–230 kW. As a result of the greater efficiency of SOFC, the unreacted hydrogen in the off-gas is lower than in other scenarios, which lessens the heating from the afterburner. Additionally, the high-temperature heating demands of the cracker and SOFC are significant. Both factors contribute to reduced available waste heat for SRC and lower electricity generation.

PEMFC has strict fuel intake requirements, particularly regarding

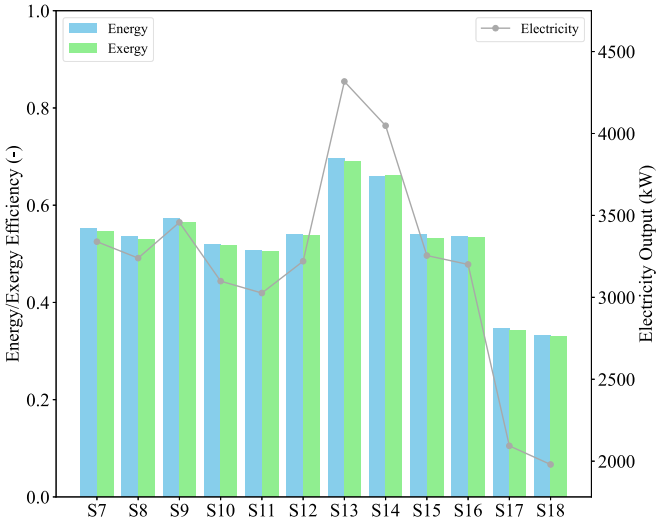

Fig. 6. Efficiency and Electricity output of different scenarios in the A2P pathway.

ammonia removal. In S7-S12, the systems maintain the same configurations as S1-S6 while incorporating a PEMFC. Because PEMFC is relatively less efficient than SOFC, the total efficiency has a maximum reduction of around 20 %. Although it produces more electricity through SRC due to a higher hydrogen content in the off-gas and a lower heating demand, this compensation is insufficient when considering the 250–420 kW range versus 2600–3200 kW from PEMFC. Systems with H2ICE in S15 and S16 have a comparable efficiency level of 53 % to that of PEMFC systems, although the efficiency of H2ICE is less than that of the fuel cells. The waste heat recovery from the exhaust largely offsets this reduction. In S17 and S18, the gas produced by the cracker is directed straight to the afterburner, which supplies the heat to power the SRC. This scenario leads to a low efficiency of about 33–34 % due to significant heat exchange.

Fig. 7 shows the breakdown of CAPEX and OPEX for scenarios in the A2P pathway, while Table 9 outlines the specific proportion of each component in the system. The system integrating H2ICE in S15 and S16 has the lowest CAPEX at 9.9 MUSD, whereas the use of SRC in S17 and S18 alone incurs the highest CAPEX at 22.4 MUSD. The largest portion of CAPEX for the system using H2ICE in S15 is attributed to SRC (25.2 %), followed by HEX (19.4 %), cracker (7.8 %), and H2ICE (6.9 %). The remaining components collectively account for less than 2 % and are negligible. The significant amount of waste heat makes the relevant costs of SRC and HEX the primary contributors to CAPEX. The cost of the cracker remains unchanged, while H2ICE makes up a small fraction of the CAPEX. This is largely due to the conservative estimation of the unit cost for H2ICE, which arises from using gasoline in the engine due to data limitations. In reality, hydrogen combustion raises concerns about NO_X emissions, flammability, material compatibility issues, and safety risks, all of which will lead to additional costs for H2ICE. Moreover, using the same amount of hydrogen results in decreased electricity output from H2ICE, resulting in a relatively smaller device requirement.

For the system directly integrating SRC in S17, the ranking is SRC (20.1 %), HEX (16.7 %), burner (12.4 %), turbine (6.8 %), and cracker (3.5 %). Nearly half of the expenses are allocated to combustion, heat exchange, and power generation. Considering the high cost of the turbine and the low system efficiency, this option is not cost-effective.

The fuel cell technologies, which demonstrate higher system efficiency, have costs that fall between using SRC alone and H2ICE. The system with SOFC incurs the second-highest CAPEX. In S13, the CAPEX is 19.9 MUSD compared to 15.8 MUSD in S8 with PEMFC. The contributions are in the order of HEX (19.3 %), fuel cell system (14.9 %), turbine (7.0 %), SRC (6.8 %), burner (6.5 %), and cracker (3.9 %). Due to the high-temperature operation of SOFC and considering the different inlet temperatures of the anode and cathode, the heat exchanger network is larger than in other systems. Additionally, the use of SRC results in an expanded heat exchange network. These factors combine to make HEX the largest contributor to CAPEX. Fuel cell systems, not just the stacks, account for nearly 15 % of the CAPEX. The stack's lifetime affects the frequency of replacement, with the stack's lifetime used in this work being 20,000 h, which is significantly less than that of H2ICE. This results in a substantial share of the CAPEX, even though the stacks represent only 21 % of the total cost.

Additionally, the unit cost presented in Table 5 is uncertain due to factors such as the number of annual manufacturing units, the size of the stack, the system size (which affects back-end costs), and the lifespan, all of which significantly influence the costs. For example, the system size correlates with unit cost, with the unit cost of a 100-kW system being half that of a 10-kW system [45]. It is crucial to note that the costs of SOFC and PEMFC used in this study are sourced from the U.S. Department of Energy, making them comparable. The PEMFC system in S8 demonstrates a reduction in costs. HEX still represents the largest share, but its ratio decreases to 14.1 %, followed by the fuel cell system at 12.9 %, the SRC at 12.6 %, the burner at 12.2 %, and the cracker at 4.9 %. Due

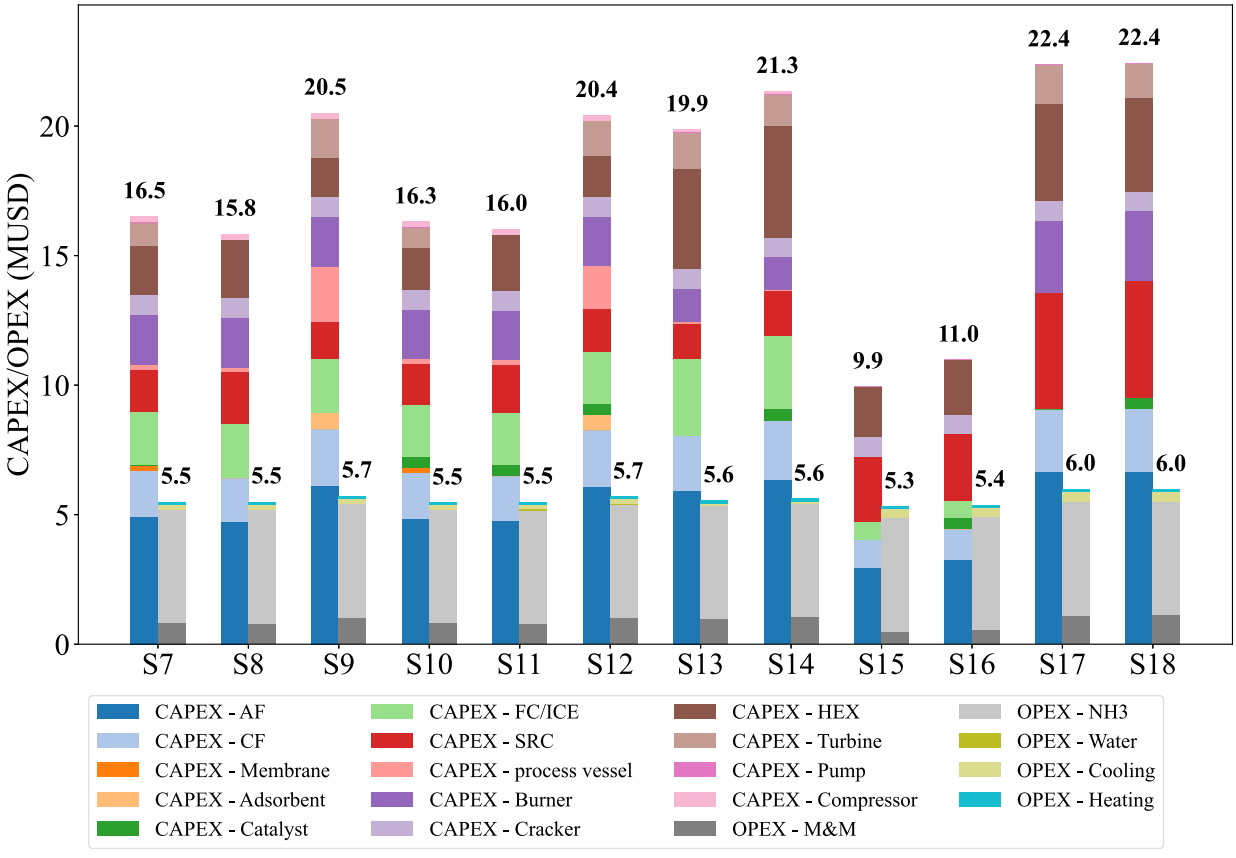

Fig. 7. Breakdown of CAPEX and OPEX of scenarios in the A2P pathway.

to the low-temperature operation of PEMFC, which is below 100 °C, the heat exchange area is minimized. The unreacted hydrogen in the off-gas is greater than that of SOFC due to efficiency, resulting in a larger burner and SRC. Utilizing SRC is less cost-effective, given the additional electricity it produces.

Fig. 8 illustrates the LCOE distribution across various scenarios within the A2P pathway, considering different ammonia prices similar to LCOH. The maximum and minimum market prices for electricity are shown at 0.09 and 0.38 USD/kWh, respectively, while the average LCOE ranges from 0.203 to 0.481 USD/kWh. The lowest LCOE, at 0.145 USD/kWh, occurs in the system employing a high-temperature cracker and SOFC without the separation and purification process in S13, while the highest LCOE, at 0.715 USD/kWh, results from the system directly integrating with SRC in S18. Due to SOFC's high efficiency, the LCOE is the lowest, differing from the CAPEX ranking.

Due to the low CAPEX of the system using H2ICE, S15 and S16 also show a competitive LCOE compared to market prices. Systems with PEMFC incur penalties from the separation and purification process, but most of the LCOE remains below the maximum market price. The LCOE for a system using hydrogen fuel cells equipped with a methanol/ammonia reformer ranges from 500 to 800 EUR/MWh, according to reference [57]. In contrast, the LCOE for a system using direct methanol/ammonia fuel cells is estimated to lie between 1000 and 1500 EUR/MWh. The primary reason for the high cost associated with direct methanol/ammonia fuel cells is their low efficiency, which stands at 42.4 % compared to 60 % for hydrogen fuel cells. The LCOE in this work is more competitive when utilizing SOFC due to the higher efficiency of the ammonia cracker and fuel cells, as well as the efficiency improvements from HEN and SRC. H2ICE is another option because of the low cost of retrofitting from existing infrastructure.

Fig. 9 illustrates the sensitivity analysis of the LCOE, measured as a function of ammonia input (kg/h) across various scenarios (S7–S18). The results indicate a sharp initial decline in LCOE with increasing ammonia input, with the slope gradually flattening beyond 2000 kg/h, signifying the elbow point where the size effect becomes less significant. In every size scenario, directly using SRC (S17 and S18) is the worst case, while utilizing the cracker integrated with SOFC is the best option due to its high efficiency. Efficiency is the most critical cost factor, particularly for a large-scale system. In a small-scale system, the system using H2ICE has a lower LCOE than most systems utilizing PEMFC, even SOFC, but a higher LCOE in a large-scale context, emphasizing the importance of efficiency.

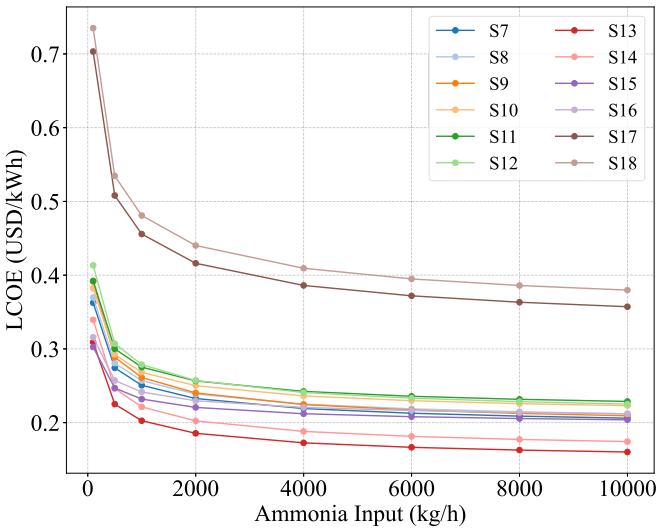

Fig. 9. LCOE distribution regarding different system sizes.

In summary, while the SOFC-based system has a higher CAPEX, its superior efficiency results in the lowest LCOE, making it the most viable option for ammonia-to-power applications. The H2ICE-based system also has a comparable LCOE due to its low CAPEX and effective heat recovery. Conversely, directly burning hydrogen in the afterburner and utilizing the heat in SRC proves to be the least efficient and cost-effective option. Efficiency is the most critical factor affecting costs in large-scale applications. Additionally, the separation and purification process in the PEMFC-based system significantly impacts both system efficiency and LCOE.

4. Conclusions

This study systematically evaluates the ammonia-to-hydrogen (A2H) and ammonia-to-power (A2P) pathways by analyzing various configurations of crackers, separation units, and power generation technologies regarding their technical and economic performance. The findings provide valuable insights into optimal design choices for hydrogen

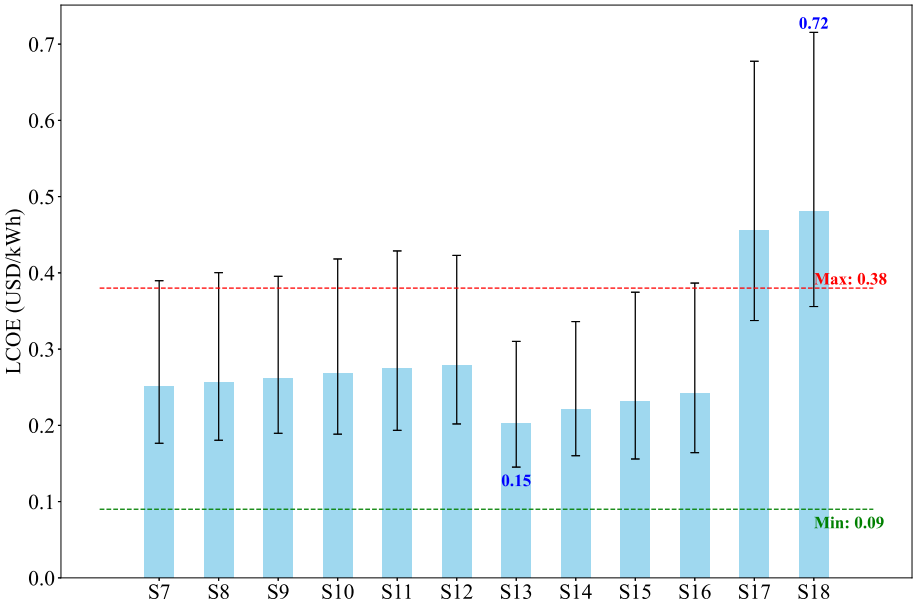

Fig. 8. LCOE distribution of different scenarios in the A2P pathway, considering different ammonia prices.

production and power generation from ammonia, considering both efficiency and cost-effectiveness.

In the A2H pathway, high-temperature crackers demonstrate superior energy and exergy efficiencies, exceeding 85 %, compared to lower-temperature crackers. This is primarily due to enhanced ammonia decomposition rates and effective energy recovery mechanisms. Among separation technologies, using TSA incurs less efficiency penalty but requires higher costs, while PSA has the lowest CAPEX and LCOH (2.81 USD/kg), rendering it a cost-effective choice despite its increased energy consumption and lower efficiency. Membrane-based separation, although having a moderate CAPEX, becomes increasingly attractive for large-scale applications because of its less energy consumption. This work also highlights the economic advantage of producing hydrogen in regions with lower electricity prices while exporting ammonia to areas with high electricity prices, facilitating a cost-effective hydrogen supply chain.

In the A2P pathway, the incorporation of fuel cell technologies significantly influences overall efficiency and economic viability. Systems employing high-temperature SOFC achieve the highest energy and exergy efficiencies, with energy efficiencies reaching up to 69.55 %. Despite their higher CAPEX, SOFC-based systems yield the lowest LCOE of 0.15 USD/kWh, making them the most viable option for A2P applications. Although integrating PEMFC or H2ICE has a lower CAPEX, they are limited by less electricity output, highlighting the essential role of efficiency enhancement. Directly burning hydrogen in an afterburner and utilizing the heat for SRC power generation results in the lowest efficiency and highest LCOE, making it the least favorable option.

Overall, this work provides a comprehensive techno-economic assessment of ammonia-based hydrogen and power production, offering valuable guidance for designing efficient and cost-effective energy systems that utilize ammonia as the energy carrier. The findings suggest that strategically deploying ammonia-based hydrogen and power technologies can facilitate a low-carbon energy transition, particularly in regions with advantageous electricity pricing structures. Future work could explore a price-driven flexible operation strategy. Given the fluctuating local market prices of hydrogen, electricity, and ammonia, the optimal scheduling of the integrated A2H and A2P systems can become more competitive. In addition, the scale-up application of the proposed scenario can be conducted to identify countries that are suitable for importing hydrogen or exporting ammonia.

CRediT authorship contribution statement

Du Wen: Writing – original draft, Methodology, Investigation, Conceptualization. **Xinyi Wei:** Writing – original draft, Methodology. **Antonin Bruneau:** Data curation. **Aris Maroonian:** Project administration. **François Maréchal:** Supervision. **Jan Van herle:** Supervision, Funding acquisition.

Declaration of competing interest

The authors declare that they have no known competing financial interests or personal relationships that could have appeared to influence the work reported in this paper.

Acknowledgments

The authors thankfully acknowledge the financial support from the project AMON. The project is supported by the Clean Hydrogen Partnership and its members under grant agreement no. 101101521. Co-funded by the European Union. Views and opinions expressed are, however, those of the author(s) only and do not necessarily reflect those of the European Union or the Clean Hydrogen Partnership. Neither the European Union nor the granting authority can be held responsible for them. This work was supported by the Swiss State Secretariat for Education, Research, and Innovation (SERI) under contract number 22.00602 - 101101521.

The authors also thankfully acknowledge the financial support from the project H2Marine. The project is supported by the Clean Hydrogen Partnership and its members under grant agreement no. 101137965. Co-funded by the European Union. Views and opinions expressed are, however, those of the author(s) only and do not necessarily reflect those of the European Union or the Clean Hydrogen Partnership. Neither the European Union nor the granting authority can be held responsible for them. This work was supported by the Swiss State Secretariat for Education, Research, and Innovation (SERI) under contract number 24.00109 - 101137965.

Finally, the authors thank the technical support and suggestions received from Neology.

Data availability

No data was used for the research described in the article.

References

[1] Wen D, Aziz M. Perspective of staged hydrogen economy in Japan: a case study based on the data-driven method. Renew Sustain Energy Rev 2024;189:113907.
[2] Lan P, Chen S, Li Q, Li K, Wang F, Zhao Y, et al. Comparison of different hydrogen-ammonia energy conversion pathways for renewable energy supply. Renew Energy 2024;227:120602.
[3] Wen D, Aziz M. Techno-economic analyses of power-to-ammonia-to-power and biomass-to-ammonia-to-power pathways for carbon neutrality scenario. Appl Energy 2022;319:119272.
[4] Cho S-H, Kim G-M, Jo H-Y, Bae Y-H, Jeon C-H. Ammonia as a hydrogen carrier: simulation study of the ammonia cracker on thermo-fluid stability and key factors for scale-up. Int J Hydrogen Energy 2024;73:148–57.
[5] Realpe N, Lezcano G, Kulkarni SR, Sayas S, Morlanes N, Rakib M, et al. The technological prospects of repurposing methane steam reformers into ammonia crackers for decarbonized H2 production. Appl Energy 2024;376:124244.
[6] Makhloufi C, Kezibri N. Large-scale decomposition of green ammonia for pure hydrogen production. Int J Hydrogen Energy 2021;46:34777–87.
[7] Park Y, Kang J-H, Moon D-K, Jo YS, Lee C-H. Parallel and series multi-bed pressure swing adsorption processes for H2 recovery from a lean hydrogen mixture. Chem Eng J 2021;408:127299.
[8] Rahimpour MR, Ghaemi M, Jokar SM, Dehghani O, Jafari M, Amiri S, et al. The enhancement of hydrogen recovery in PSA unit of domestic petrochemical plant. Chem Eng J 2013;226:444–59.
[9] Vo D-N, Hun Chang J, Hong S-H, Lee C-H. Comparative performance and machine learning-based optimization of TSA configurations for NH3 removal from NH3 cracking gas. Chem Eng J 2023;475:146195.
[10] Golmakani A, Fatemi S, Tamnanloo J. Investigating PSA, VSA, and TSA methods in SMR unit of refineries for hydrogen production with fuel cell specification. Sep Purif Technol 2017;176:73–91.
[11] Jo YS, Cha J, Lee CH, Jeong H, Yoon CW, Nam SW, et al. A viable membrane reactor option for sustainable hydrogen production from ammonia. J Power Sources 2018;400:518–26.
[12] Wei Q, Lucero JM, Crawford JM, Way JD, Wolden CA, Carreon MA. Ammonia separation from N2 and H2 over LTA zeolitic imidazolate framework membranes. J Membr Sci 2021;623:119078.
[13] Wang B, Wang H, Duan B, Yang C, Hu D, Wang Y. Effect of ammonia/hydrogen mixture ratio on engine combustion and emission performance at different inlet temperatures. Energy 2023;272:127110.
[14] Pankratov S, Dimitriou P, Sheintuch M, Tartakovsky L. Exploring the potential of urea reforming in internal combustion engines. Fuel 2025;381:133420.
[15] Richard S, Ramirez Santos A, Olivier P, Gallucci F. Techno-economic analysis of ammonia cracking for large scale power generation. Int J Hydrogen Energy 2024;71:571–87.
[16] Cesaro Z, Ives M, Nayak-Luke R, Mason M, Bañares-Alcántara R. Ammonia to power: forecasting the levelized cost of electricity from green ammonia in large-scale power plants. Appl Energy 2021;282:116009.
[17] Bertran M-O, Frauzem R, Sanchez-Arcilla A-S, Zhang L, Woodley JM, Gani R. A generic methodology for processing route synthesis and design based on superstructure optimization. Comput Chem Eng 2017;106:892–910.
[18] Wan Z, Tao Y, Shao J, Zhang Y, You H. Ammonia as an effective hydrogen carrier and a clean fuel for solid oxide fuel cells. Energ Conver Manage 2021;228:113729.
[19] Mukelabai MD, Gillard JM, Patchigolla K. A novel integration of a green power-to-ammonia to power system: reversible solid oxide fuel cell for hydrogen and power production coupled with an ammonia synthesis unit. Int J Hydrogen Energy 2021;46:18546–56.
[20] Al-Hamed KHM, Dincer I. A novel ammonia solid oxide fuel cell-based powering system with on-board hydrogen production for clean locomotives. Energy 2021;220:119771.
[21] Rathore SS, Biswas S, Fini D, Kulkarni AP, Giddey S. Direct ammonia solid-oxide fuel cells: a review of progress and prospects. Int J Hydrogen Energy 2021;46:35365–84.

[22] Sánchez A, Castellano E, Martín M, Vega P. Evaluating ammonia as green fuel for power generation: a thermo-chemical perspective. Appl Energy 2021;293:116956.
[23] Peng P, Su J, Breunig H. Benchmarking plasma and electrolysis decomposition technologies for ammonia to power generation. Energ Conver Manage 2023;288:117166.
[24] Elmutasim O, Giddey S, Dhawale DS, Bhattacharya S. Ammonia to power: advancing direct ammonia solid oxide fuel cells through experimental and theoretical studies. Int J Hydrogen Energy 2024;96:192–209.
[25] Pinzón M, García-Carpintero R, de la Osa AR, Romero A, Abad-Correa D, Sánchez P. Ammonia as a hydrogen carrier: an energy approach. Energ Conver Manage 2024;321:118998.
[26] Mucci S, Stumm M-D, Rix MJ, Mitsos A. Model-based evaluation of ammonia energy storage concepts at high technological readiness level. Appl Energy 2025;377:124495.
[27] Wen D, Liu SC, Ning ZY, Aziz M. Techno-economic evaluation of hydrogen and ammonia as energy carriers in a multi-generation system. Energ Conver Manage 2023;277:116670.
[28] Wen D, Aziz M. Design and analysis of biomass-to-ammonia-to-power as an energy storage method in a renewable multi-generation system. Energ Conver Manage 2022;261:115611.
[29] Asif M, Sidra Bibi S, Ahmed S, Irshad M, Shakir Hussain M, Zeb H, et al. Recent advances in green hydrogen production, storage and commercial-scale use via catalytic ammonia cracking. Chem Eng J 2023;473:145381.
[30] Aspen Technology, Inc.. ASPEN Plus, Version 11.1. Aspen Technology; 2024. www.aspentech.com.
[31] Zhang Z, Liguori S, Fuerst TF, Way JD, Wolden CA. Efficient Ammonia decomposition in a catalytic membrane reactor to enable hydrogen storage and utilization. ACS Sustain Chem Eng 2019;7:5975–85.
[32] Micari M, Agrawal KV. Oxygen enrichment of air: performance guidelines for membranes based on techno-economic assessment. J Membr Sci 2022;641:119883.
[33] Pal N, Agarwal M. Advances in materials process and separation mechanism of the membrane towards hydrogen separation. Int J Hydrogen Energy 2021;46:27062–87.
[34] Yáñez M, Ortiz A, Gorri D, Ortiz I. Comparative performance of commercial polymeric membranes in the recovery of industrial hydrogen waste gas streams. Int J Hydrogen Energy 2021;46:17507–21.
[35] Shen C, Qiu H, Guo W. Ultrahigh hydrogen and nitrogen selectivity achieved by the nanoporous graphene with a precise nanopore. Carbon 2021;182:628–33.
[36] Takahashi T, Ikeda T, Murata K, Hotaka O, Shigeki H, Tachikawa Y, et al. Accelerated durability testing of fuel cell stacks for commercial automotive applications: a case study. J Electrochem Soc 2022;169:044523.
[37] Wen D, Aziz M. Flexible operation strategy of an integrated renewable multi-generation system for electricity, hydrogen, ammonia, and heating. Energ Conver Manage 2022;253:115166.
[38] Chen D, Pei P, Ren P, Song X, Wang H, Zhang L, et al. Analytical methods for the effect of anode nitrogen concentration on performance and voltage consistency of proton exchange membrane fuel cell stack. Energy 2022;258:124850.
[39] Wei X, Sharma S, Van herle J, Maréchal F. Efficient, affordable, carbon-neutral power: advanced solid oxide fuel cell-electrolyzer system. Renew Sustain Energy Rev 2025;211:115328.
[40] Lago Sari R, Fogue Robles A, Monsalve Serrano J, Cleary D. Techno-economic assessment of hydrogen as a fuel for internal combustion engines and proton exchange membrane fuel cells on long haul applications. Energ Conver Manage 2024;311:118522.
[41] Mian A, Martelli E, Maréchal F. Framework for the multiperiod sequential synthesis of heat exchanger networks with selection, design, and scheduling of multiple utilities. Ind Eng Chem Res 2016;55:168–86.
[42] Nguyen TV, Lock L, Breuhaus P, Maréchal F, Elmegaard B. Oil and gas platforms with steam bottoming cycles: system integration and thermoenvironomic evaluation. Appl Energy 2014;131:222–37.
[43] Bendig M, Maréchal F, Favrat D. Defining "waste heat" for industrial processes. Appl Therm Eng 2013;61:134–42.
[44] U.S.D.o. Energy. Manufacturing cost analysis of PEM fuel cell systems for 5- and 10-kW backup power applications. 2016.
[45] U.S.D.o. Energy. A total cost of ownership model for solid oxide fuel cells in combined heat and power and power-only applications. 2015.
[46] U.S. Energy Information Administration (EIA). Cost and Performance Characteristics of New Generating Technologies, Annual Energy Outlook. Available at: https://www.eia.gov/electricity/generatorcosts/; 2022.
[47] Alkandari SH, Castro-Dominguez B. Advanced and sustainable manufacturing methods of polymer-based membranes for gas separation: a review. Front Membr Sci Technol 2024;3.
[48] Tran TV, Oni AO, Gemechu E, Carrier Y, Tezel FH, Kumar A. Developing a techno-economic model to evaluate the cost performance of a zeolite 13X-based space heating system. Energ Conver Manage 2021;244:114325.
[49] Turton R, Shaeiwitz JA, Bhattacharyya D, Whiting WB. Analysis, synthesis, and design of chemical processes. Pearson Education; 2018.
[50] Ravi M, Makepeace JW. Facilitating green ammonia manufacture under milder conditions: what do heterogeneous catalyst formulations have to offer? Chem Sci 2022;13:890–908.
[51] U.S. Energy Information Administration, Form EIA-861M (formerly EIA-826), Monthly Electric Power Industry Report. Access date: 2024. Available at: https://www.eia.gov/electricity/monthly/epm_table_grapher.php?t=epmt_5_6_a. .
[52] Styles C. Revisiting the Costs of Nitrogen Gas. Available at: https://puritygas.ca/revisiting-the-costs-of-nitrogen-gas/; 2022.
[53] Faouzi Aloulou PG, Lorenz Thomas, O'Sullivan Jim. U.S. refiners and chemical manufacturers lead hydrogen production and consumption. Available at: https://www.eia.gov/todayinenergy/detail.php?id=61763.
[54] Apodaca LE. Ammonia - mineral commodity summaries. Available at: https://pubs.usgs.gov/periodicals/mcs2024/mcs2024-nitrogen.pdf; 2024.
[55] Consumer Price Index. Available at: https://www.minneapolisfed.org/about-us/monetary-policy/inflation-calculator/consumer-price-index-1913-; 1913.
[56] IEA. Global Hydrogen Review 2021. Paris: IEA; 2021. https://www.iea.org/reports/global-hydrogen-review-2021. Licence: CC BY 4.0.
[57] Sánchez A, Blanco EC, Martín M. Comparative assessment of methanol and ammonia: green fuels vs. hydrogen carriers in fuel cell power generation. Appl Energy 2024;374:124009.